Article

Cell Reports

A CEP104-CSPP1 Complex Is Required for Formation of Primary Cilia Competent in Hedgehog Signaling

Graphical Abstract

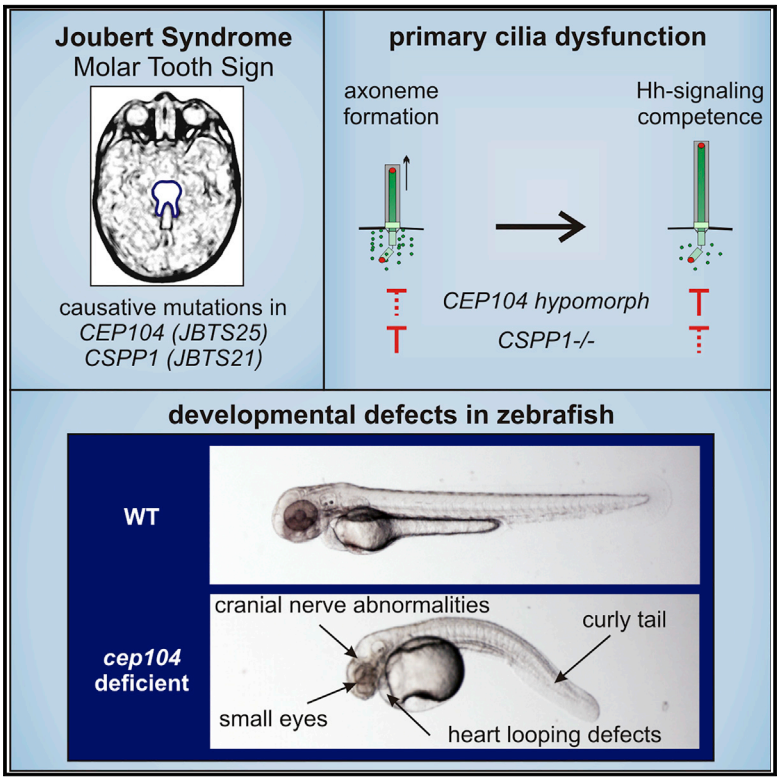

Highlights

- cep104-depleted zebrafish display shortened KV cilia and defective brain development
- CEP104 interacts with CSPP1 at the tip of the primary cilium to regulate cilia length
- CEP104 or CSPP1 loss in human cells leads to defective Hedgehog signaling
- Impaired signaling is linked to reduction of ciliary SMO but not ARL13B or INPP5E

Authors

Kari-Anne M. Frikstad, Elisa Molinari, Marianne Thoresen, ..., Ronald Roepman, John A. Sayer, Sebastian Patzke

Correspondence

sebastip@rr-research.no

In Brief

Deleterious mutations in *CEP104* or *CSPP1* cause Joubert syndrome, a ciliopathy causing an underdeveloped mid- and/or hindbrain. Frikstad et al. show that loss of cep104 in zebrafish leads to defective brain development and that CEP104 interacts with CSPP1 at the tip of the primary cilium to regulate axoneme length and Hedgehog signaling competence.

Frikstad et al., 2019, Cell Reports *28*, 1907–1922
August 13, 2019
https://doi.org/10.1016/j.celrep.2019.07.025

CellPress

Cell Reports
Article

A CEP104-CSPP1 Complex Is Required for Formation of Primary Cilia Competent in Hedgehog Signaling

Kari-Anne M. Frikstad,[1] Elisa Molinari,[2] Marianne Thoresen,[1] Simon A. Ramsbottom,[2] Frances Hughes,[2] Stef J.F. Letteboer,[3] Sania Gilani,[1] Kay O. Schink,[4] Trond Stokke,[1] Stefan Geimer,[5] Lotte B. Pedersen,[6] Rachel H. Giles,[7] Anna Akhmanova,[8] Ronald Roepman,[3] John A. Sayer,[2,9,10] and Sebastian Patzke[1,11,*]

[1]Department of Radiation Biology, Institute for Cancer Research, OUH-Norwegian Radium Hospital, Oslo, Norway
[2]Newcastle University, Institute of Genetic Medicine, International Centre of Life, Newcastle upon Tyne NE1 3BZ, UK
[3]Department of Human Genetics and Radboud Institute for Molecular Life Sciences, Radboud University Medical Center, Nijmegen, the Netherlands
[4]Department of Molecular Cell Biology, Institute for Cancer Research, OUH-Norwegian Radium Hospital, Oslo, Norway
[5]Cell Biology/Electron Microscopy, University of Bayreuth, Bayreuth, Germany
[6]Department of Biology, University of Copenhagen, Copenhagen, Denmark
[7]Department of Nephrology and Hypertension, Regenerative Medicine Center Utrecht, University Medical Center Utrecht, Utrecht, the Netherlands
[8]Department of Cell Biology, Faculty of Science, Utrecht University, Utrecht, the Netherlands
[9]The Newcastle upon Tyne NHS Foundation Trust, Freeman Road, Newcastle NE7 7DN, UK
[10]Biomedical Research Centre, Newcastle upon Tyne NE4 5PL, UK
[11]Lead Contact
*Correspondence: sebastip@rr-research.no
https://doi.org/10.1016/j.celrep.2019.07.025

SUMMARY

CEP104 is an evolutionarily conserved centrosomal and ciliary tip protein. *CEP104* loss-of-function mutations are reported in patients with Joubert syndrome, but their function in the etiology of ciliopathies is poorly understood. Here, we show that *cep104* silencing in zebrafish causes cilia-related manifestations: shortened cilia in Kupffer's vesicle, heart laterality, and cranial nerve development defects. We show that another Joubert syndrome-associated cilia tip protein, CSPP1, interacts with CEP104 at microtubules for the regulation of axoneme length. We demonstrate in human telomerase reverse transcriptase-immortalized retinal pigmented epithelium (hTERT-RPE1) cells that ciliary translocation of Smoothened in response to Hedgehog pathway stimulation is both CEP104 and CSPP1 dependent. However, CEP104 is not required for the ciliary recruitment of CSPP1, indicating that an intra-ciliary CEP104-CSPP1 complex controls axoneme length and Hedgehog signaling competence. Our *in vivo* and *in vitro* analyses of CEP104 define its interaction with CSPP1 as a requirement for the formation of Hedgehog signaling-competent cilia, defects that underlie Joubert syndrome.

INTRODUCTION

The primary cilium is a signaling organelle formed by a confined microtubule (MT)-based cell membrane protrusion that originates from the modified mother centriole of the centrosome (basal body). Generation of a signaling-competent primary cilium from the centrosome is a multi-step process. It is initiated by the re-organization of the distal end of the mother centriole and the recruitment of pre-ciliary membrane, and completed by docking to the cell membrane and maturation of the ciliary axoneme and membrane. A highly specialized region at the base of the MT axoneme, the transition zone (TZ), regulates the exchange of membrane-bound and soluble cytosolic factors with the cell body (Reiter et al., 2012). Ciliary compartmentalization is further regulated by the intraflagellar transport system (IFT), which mediates anterograde (base to tip) with IFT-B cargo via kinesin-2 and retrograde (tip to base) with IFT-A complex-bound cargo via dynein 2 motors (Taschner and Lorentzen, 2016). Kinesin-2 motors and the IFT-B sub-complex are known to promote ciliogenesis via the anterograde ciliary transport of soluble axonemal cargoes such as tubulin (Kozminski et al., 1995; Bhogaraju et al., 2013). Emerging evidence has implicated IFT-A also in the ciliary entrance of specific G protein-coupled receptors via Tubby family adaptor proteins (Mukhopadhyay et al., 2010; Pal et al., 2016), and IFT-B complex members and dynein 2 motors were shown to promote the ciliary export of specific membrane proteins, such as the Sonic hedgehog (SHH) signaling pathway receptors Patched1 and Smoothened (Keady et al., 2012; Eguether et al., 2014), via the Bardet-Biedl syndrome protein complex (BBSome), an IFT cargo adaptor (Lechtreck, 2015; Nachury, 2018). The restricted ciliary expression of receptor molecules allows cell surface area-independent sensitivity to surrounding ligands and orientation-dependent signal reception within a tissue context (Mahjoub, 2013). Several key pathways in vertebrate development and tissue homeostasis depend on primary cilia, including Hedgehog (Hh), WNT, transforming growth factor β (TGF-β) and platelet-derived growth factor

receptor α (PDGFR-α) signaling (Bangs and Anderson, 2017; Christensen et al., 2017; May-Simera and Kelley, 2012). Structural and/or functional cilium defects conferred by inherited mutations in ciliary and/or centrosomal protein-encoding genes are acknowledged as a leading cause of developmental disorders and degenerative diseases, collectively called ciliopathies (Waters and Beales, 2011; Reiter and Leroux, 2017). Affected individuals typically present with multi-system pathologies of the brain and/or neurological system, eye, kidney, skeleton, and other organs relying on ciliary signaling and function.

Joubert syndrome (JBTS) is a rare autosomal recessive ciliopathy classified by a characteristic mal-development of the mid- and/or hindbrain (manifesting as a "molar tooth sign" on brain MRI). Besides developmental delay, ataxia, and intellectual disabilities, retinal dystrophy and cystic kidney disease (nephronophthisis, NPHP) frequently co-occur (Romani et al., 2013). To date, JBTS-causing mutations have been identified in 35 genes (JBTS1–JBTS35; MIM Phenotypic series MIM: PS213300), partially overlapping with related ciliopathies such as Meckel-Gruber syndrome (MKS), Senior-Løken syndrome (SLSN), BBS, and NPHP (Sang et al., 2011). The majority of JBTS genes have been tied to the regulation of the Hh signaling pathway and function of the TZ (Garcia-Gonzalo et al., 2011; Yang et al., 2015; Chih et al., 2011). A subset of four JBTS proteins localizes to the ciliary tip, and these proteins have opposing effects on cilium structure: cells depleted of KIF7 (JBTS12) or KIAA0556 (JBTS26) have extended axonemes (He et al., 2014; Dafinger et al., 2011; Sanders et al., 2015), as opposed to cells with reduced CSPP1 (JBTS21) or CEP104 (JBTS25), which manifest shortened or absent axonemes (Patzke et al., 2010; Akizu et al., 2014; Shaheen et al., 2014; Tuz et al., 2014; Satish Tammana et al., 2013; Jiang et al., 2012). Of note, the cilia phenotype of *CEP104* mutation carriers has not yet been reported, nor has genetic silencing been tested in vertebrate models. Studies in human telomerase reverse transcriptase-immortalized retinal pigmented epithelium (hTERT-RPE1) cells revealed that CEP104 interacts with MT plus end-tracking (EB1/EB3) and centriolar capping complex (CEP97/CP110) proteins (Jiang et al., 2012). CEP104 is lost from the mother centriole upon the induction of ciliogenesis and localizes to the tip of the axoneme (Satish Tammana et al., 2013; Jiang et al., 2012). Recent structural analyses and interaction studies defined a tubulin-binding chTOG domain in the central part of CEP104 and an NEK1/CP110 binding zinc-finger array in its C-terminal domain (Rezabkova et al., 2016; Al-Jassar et al., 2017). However, axonemal interaction partners of CEP104 remain elusive.

Here, we report ciliopathy-associated developmental defects in *cep104*-targeted zebrafish and identify CSPP-L, the large and predominantly expressed *CSPP1 (JBTS21)* splice isoform (Patzke et al., 2010), as a direct interaction partner of CEP104. The characterization of CEP104 and CSPP-L in genetically engineered hTERT-RPE1 cell line models determines the interaction of these ciliary tip proteins as a requirement for Hh signaling-competent axoneme formation. Our *in vivo* and *in vitro* studies tie CEP104 physically and functionally to the existing JBTS protein network and provide a pathogenic basis for *CEP104* mutations in humans with JBTS.

RESULTS

Ciliary Defects and Ciliopathy Phenotypes in *cep104* Zebrafish Morphants

CEP104 is a highly conserved gene in ciliated organisms (Figures S1A–S1D) for which deleterious mutations were reported in JBTS patients (Srour et al., 2015). *CEP104* function has not yet been interrogated in vertebrate development, and CEP104 has not previously been shown to physically interact with components of the JBTS protein network. To study the effect of cep104 depletion in *Danio rerio* (zebrafish), we injected morpholino oligonucleotides targeting the single ortholog *cep104* at the translation site (*cep104* translation blocking morpholino oligonucleotide [ATG MO]) and a splice junction (*cep104* splice MO). Morphant zebrafish at 48 h post fertilization (hpf) displayed cardiac phenotypes, mild tail curvature, and microophthalmia (Figures 1A–1C and S2A–S1C). The combined injection of *cep104* ATG MO and *cep104* splicing MO potentiated the severity of morphant phenotypes (Figure 1D). RT-PCR and western blotting of whole zebrafish mRNA and/or protein revealed aberrant *cep104* RNA splicing and significant protein knockdown of cep104 in 48 hpf morphant embryos (Figures 1E and S2D). The gross morphological changes could be rescued by co-injection of human *CEP104* mRNA (Figure S2E), confirming the specificity of the morpholinos. Immunofluorescence microscopy (IFM) of the pronephros revealed no obvious cilia defects (Figure S2F). In contrast, analysis of Kupffer's vesicle, a ciliated organelle important for left-right axis formation, showed a ciliary defect, with a reduction in ciliary length (Figures 1F and 1G), which was rescued by the co-administration of *CEP104* mRNA. In addition to pericardial edema, which was not directly related to laterality defects, cardiac defects included abnormal cardiac looping, with reversed or no looping seen in 55% of morphants, which was also rescued by co-injection with *CEP104* mRNA (Figures 1H and 1I). Most relevant in regard to JBTS, characteristic developmental defects were observed within the brains of *cep104* zebrafish morphants. The transgenic zebrafish line, *islet1*-GFP, allows visualization of the cranial motor neurons. In morphant embryos, *islet1*-GFP positivity was disrupted with the loss of the overall neuronal structure and with a specific, recurrent loss of oculomotor neurons. Notably, the degree of cranial nerve defect did not necessarily correlate with the severity in body structure abnormalities, indicating that the neuronal phenotype is not secondary to a more general developmental defect. This specific phenotype was rescued by co-administration of *CEP104* mRNA (Figures 1J and 1K). Additional analysis of the F0 populations of *cep104* crispants confirmed the specificity of the gross morphological changes, as well as the heart looping, Kupffer's vesicle cilia, and cranial nerve defects seen in *cep104* morphants (Figures S2G–S2Q). Severe crispants and morphants showed some yolk sac abnormalities, which are likely to be linked to the pericardial edema. These data reveal that *cep104* knockdown phenotypes are highly consistent with a ciliopathy syndrome and suggest a role for cep104 in cilia formation within Kupffer's vesicle, as well as development of the heart and cranial nerves in zebrafish.

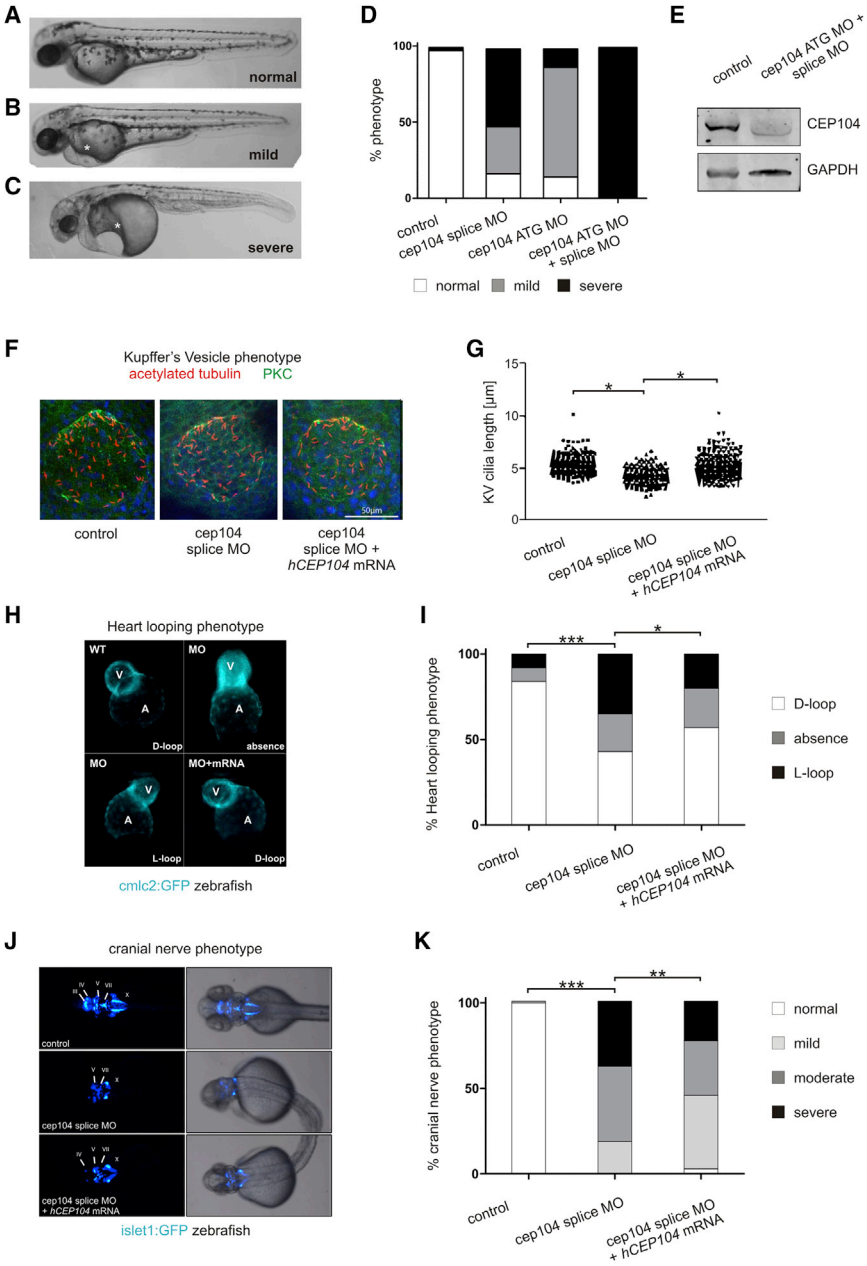

Figure 1. *cep104* Knockdown in Zebrafish Embryos Leads to Ciliopathy Phenotypes

(A–C) 48 hpf morphant zebrafish display mild and severe pericardial edema and cardiac defects (*) following *cep104* knockdown and additional phenotypes in severe morphants of mild tail curvature and microopthalmia, with a quantified reduction in area expressed as a ratio to control embryos of 0.45 ($p < 0.0001$, unpaired t test, n = 39 versus 28 control).

(D) Percentage of zebrafish displaying phenotypes following injection of *cep104* splice MO and translation blocking morpholino *cep104* ATG MO alone or in combination (control n = 98, *cep104* splice MO n = 166, *cep104* ATG MO n = 95, *cep104* splice MO + *cep104* ATG MO n = 77).

(E) Western blotting (WB) of cep104 at 48 hpf in zebrafish uninjected and injected with *cep104* ATG MO and *cep104* splice MO.

(F) IFM of cilia and cell junctions (a-acetylated tubulin, red) in Kupffer's vesicle (KV; atypical protein kinase C [aPKC], green) at the 10-somite stage in control and *cep104* knockdown embryos.

(G) Dot plots of the length of cilia in KV in control, *cep104* splice MO knockdown, and *cep104* splice MO and *CEP104* mRNA co-injected zebrafish embryos (ANOVA with Tukey post hoc test, $*p < 0.05$).

(H) 48 hpf *cmlc2*:GFP zebrafish treated with *cep104* splice MO show changes to heart looping at 48 hpf, which is rescued by co-injection with *CEP104* mRNA.

(I) Percentage of embryos displaying heart looping phenotypes following injection of *cep104* splice MO and co-injection with *CEP104* mRNA (***$p < 0.0001$, *$p = 0.0208$, chi-square test of independence; control n = 186; *cep104* splicing MO n = 132; *cep104* splicing MO + *CEP104* mRNA n = 130).

(J and K) *cep104* knockdown in 48 hpf *islet-1*:GFP transgenic fish leads to cranial nerve defects, rescued by co-injection with *CEP104* mRNA. Co-injection with *CEP104* mRNA produces a partial rescue of phenotypes (***$p < 0.0001$, **$p = 0.0010$, chi-square test of independence; control n = 200; *cep104* splicing MO n = 80; *cep104* splicing MO + *CEP104* mRNA n = 120).

Identification of Microtubule-Associated CEP104-CSPP-L Complexes

A key to understanding the underlying mechanism of the zebrafish phenotype is to place CEP104 within known ciliopathy-associated protein networks. We identified an interaction of CEP104 with the JBTS protein CSPP-L (the larger and predominantly expressed isoform of *CSPP1*) in a bi-directional yeast two-hybrid screen of an arrayed cDNA panel encoding 163 ciliary proteins or protein fragments (Table S1; Figures S3A–S3D). This finding was supported by BirA(R118G)-CEP104 proximity labeling studies in Hek293 cells (Al-Jassar et al., 2017; Gupta et al., 2015), as well as co-fractionation of endogenous proteins in hTERT-RPE1 and Hek293T cells during sucrose gradient centrifugation and size exclusion chromatography (Figures S3E and S3F). We validated the interaction of CSPP-L and CEP104 in reciprocal co-immunoprecipitation experiments using EGFP-tagged CEP104 and CSPP-L full-length or truncated constructs (Figures 2A–2C). The localization pattern of the N-terminally fluorescent protein-tagged CEP104 to the distal end of centrioles and the cilia axoneme, and to some extent MT plus ends, closely resembles that reported for endogenous CEP104 (Figures S3G and S3H; Satish Tammana et al., 2013; Jiang et al., 2012). CSPP-L and known CEP104-interacting proteins CEP97, CP110, and CEP290 co-purified with EGFP-CEP104.

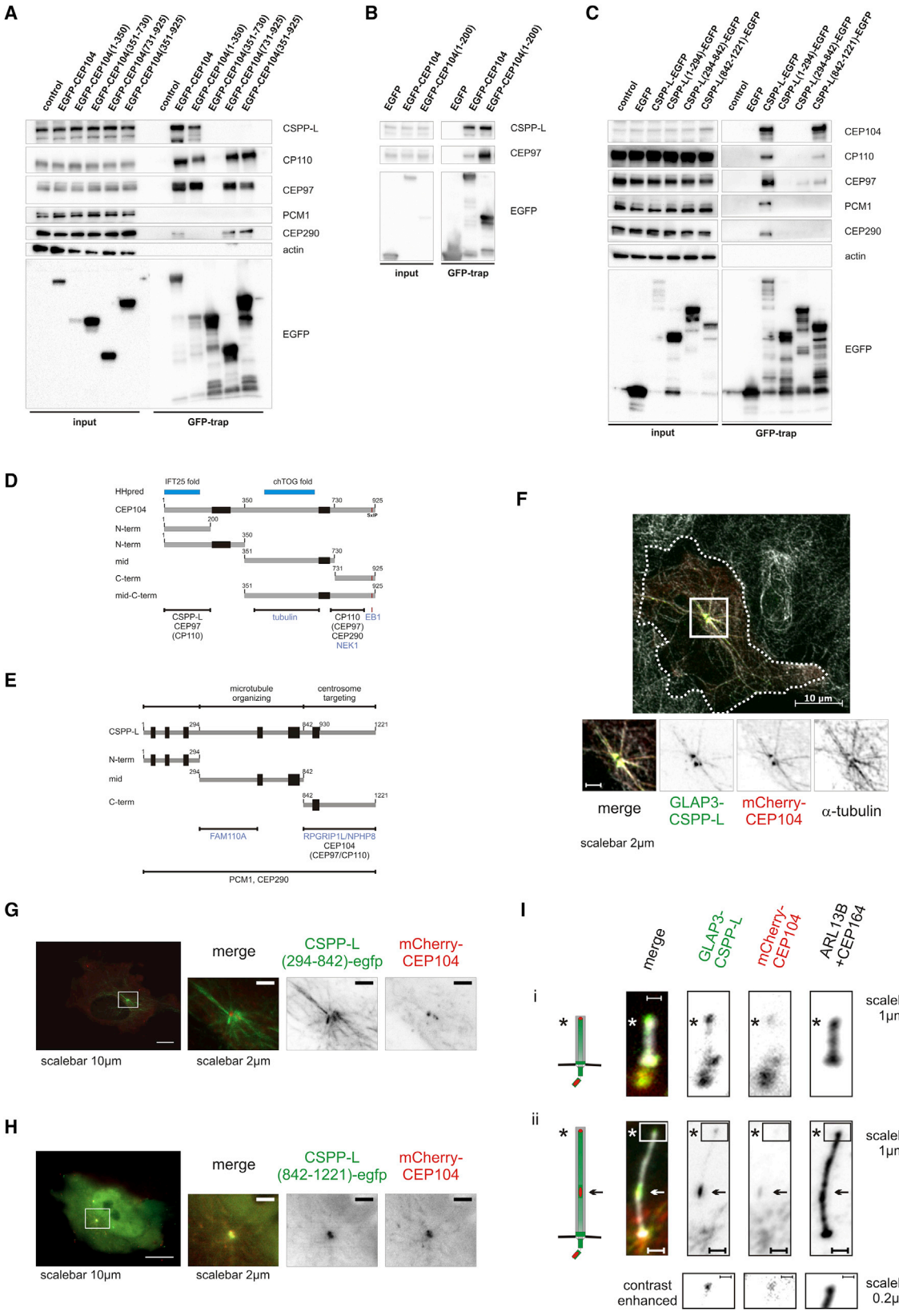

(legend on next page)

Analysis of truncation mutants identified the N-terminal 200 amino acid domain of CEP104 as being essential for interaction with CSPP-L (Figures 2A and 2B). Conversely, CSPP-L-EGFP specifically co-purified with endogenous CEP104 and CEP97, CP110, and the earlier identified CSPP-L interaction partners CEP290 and PCM1 (Figure 2C; Patzke et al., 2005, 2012; Shearer et al., 2018). The co-purification of CSPP-L with CEP104, CEP97, and CP110 was strictly dependent on the C-terminal 379 amino acid of CSPP-L. CSPP-L truncates failed to co-purify CEP290 or PCM1, which may indicate the requirement of a distinct tertiary fold of CSPP-L for stable interaction with these centriolar satellite proteins. In line with subcellular localization data, PCM1 co-purified only with CSPP-L-EGFP but not EGFP-CEP104 (Figures 2A, 2C, S5A, and S5B). CSPP-L may thus participate in distinct sub-complexes. Figures 2D and 2E summarize the biochemical data and superimpose protein partner interacting regions of CSPP-L and CEP104 on their functional (Patzke et al., 2005, 2006, 2010, 2012; Jiang et al., 2012; Hauge et al., 2007) and predicted domain architectures (Hildebrand et al., 2009; Meier and Söding, 2015). Bioinformatic analysis of CSPP-L did not identify regions of significant structural homology to functionally annotated proteins. In contrast, the N-terminal galactose-binding-like domain of CEP104 (amino acids [aa] 1–156) is predicted to share close structural homology to the Hh signaling pathway regulating IFT-B complex protein IFT25 (Keady et al., 2012), and the central domain (aa439-658) is homologous to a single ch-TOG domain of proteins involved in MT plus end dynamics (Al-Jassar et al., 2017; Al-Bassam and Chang, 2011; Akhmanova and Steinmetz, 2015).

We noticed earlier that the localization of CSPP-L to MTs is spatiotemporally restricted to the cilia axoneme and mitotic MTs and otherwise generally confined to centrosomes and centriolar satellites (Patzke et al., 2010; Shearer et al., 2018). Hence, the interaction of endogenous CSPP-L with MTs may depend on post-translational modification and/or require a secondary factor. Overexpressed CSPP-L, however, decorates cytoplasmic MTs (Patzke et al., 2006, 2010). Co-expression of mCherry-CEP104 with GLAP3-CSPP-L or its truncated variants CSPP-L(294–842)-EGFP or CSPP-L(842–1,221)-EGFP (described in Patzke et al., 2006) in non-ciliated hTERT-RPE1 cells revealed the recruitment of mCherry-CEP104 to cytoplasmic MTs. This recruitment was dependent on the CEP104 interacting C-terminal domain of CSPP-L (Figures 2F–2H, S3I, and S3J). CSPP-L may thus support the localization of CEP104 to MTs in the cilium to facilitate axoneme formation and/or stabilization. GLAP3-CSPP-L and mCherry-CEP104 partially co-localized at the ciliary tip in transient hTERT-RPE1 transfectants (Figure 2I).

Ciliary Localization of CSPP-L and CEP104

The IFM analyses described above supported an MT-associated function of CSPP-L and CEP104 at the ciliary axoneme and/or tip, but they were limited by the transient overexpression of CSPP-L and CEP104 fusion proteins. To refine the ciliary localization at a higher resolution, we resolved the localization of endogenous CSPP-L by IFM and electron microscopy on multiciliated mouse trachea epithelia cells and of N-terminal monomeric NeonGreen fluorescent protein fusions of CSPP-L (mNG-CSPP-L) and CEP104 (mNG-CEP104) by 3D-superresolution immunofluorescence microscopy (3D-SIM) in transformed hTERT-RPE1 cells (Figures 3 and 4). CSPP-L localizes predominantly to the very end of axonemal MTs near the capping structure (Figures 3A and 3B) and to the membrane proximal end of the transition fibers of motile cilia in mouse trachea cells (Figure 3A). The axoneme end localization is more proximal to the cilia tip than that of the apical membrane-singlet MT linker protein Sentan (Figure 3C) (Kubo et al., 2008). CSPP-L staining along outer and central axonemal MTs was occasionally observed (Figure 3A). In addition, staining of electron-dense particles, tentative centriolar satellites, was noticed (Figure 3A). Notably, MT end localization was not seen in the axonemes of mouse sperm flagella (Figure S4A) or the cytoplasmic MTs of hTERT-RPE1 cells (Figure S4B). mNG-CSPP-L closely resembled the localization pattern of endogenous CSPP-L in hTERT-RPE1 cells, including centriolar satellite localization (Figures 3D, 3E, and S4C; Patzke et al., 2010). mNG-CSPP-L is partially co-localized with the central dot of γ-tubulin (centriole lumen; Lawo et al., 2012) of both centrioles. It extends from the mother centriole through the TZ into the cilia lumen to peak in intensity at the ARL13B encased tip (Figure S4D), distal to the antibody-stained glutamylated MT axoneme. mNG-CEP104 localizes to the cilia tip and the distal end of the daughter centriole (Figures 4 and S4E). The cilia tip localization with respect to ARL13B (Figures 4A and 4B) and glutamylated tubulin (Figures 4C and 4D) is highly reminiscent of CSPP-L, and partial co-localization of CSPP-L and mNG-CEP104 is evident (Figure 4C). mNG-CEP104 partially co-localizes with CP110 at the distal end of

Figure 2. Interaction and MT-Associated Co-localization of CEP104 and CSPP-L

(A–C) Immunodetection of indicated endogenous centrosomal and/or ciliary proteins co-purified with full-length or truncated GFP-tagged CEP104 (A and B) and CSPP-L variants (C). GFP-fusion proteins were expressed in Hek293T cells and purified using paramagnetic GFP-trap beads. The N-terminal CEP104-domain (aa 1–200) confers interaction with the C-terminal CSPP-L (aa 842–1,221) domain. CSPP-L but not CEP104 co-purifies PCM1.

(D and E) Schematic drawing of CEP104 (D) and CSPP-L (E) proteins and tested truncation variants, including functional domains and allocated interaction partners identified here and previously (Huage et al., 2007; Patzke et al., 2010; Jiang et al., 2012). Predicted coiled-coil domains (UniProt) are indicated as black boxes. Bio-informatic analysis identifies structural homologies (blue boxes) to IFT25 (CEP104 aa 1–158 to hIFT25 aa 17–151: probability 99.9%; E value 1.1E−21, p value 7.2E−27) and a single chTOG domain (CEP104 aa 415–637 to hCLASP aa 28–266: probability 99.7%; E value 2E−15, p value 1.3E−20).

(F) IFM of hTERT-RPE1 cells transiently expressing mCherry-CEP104 (red) and GLAP3-CSPP-L (green) and co-stained for α-tubulin (a-acetylated-tubulin, white). At increasing expression levels, mCherry-CEP104 and GLAP3-CSPP-L decorate centrosome originating MTs (see also Figure S4).

(G and H) Live cell microcopy of hTERT-RPE1 cells co-transfected with mCherry-CEP104 and CSPP-L(294-842)-EGFP (G) or CSPP-L(842-1221)-EGFP (H), respectively, showing dependence on the C-terminal domain of CSPP-L for the recruitment of mCherry-CEP104 along microtubules.

(I) IFM of hTERT-RPE1 cells transiently expressing mCherry-CEP104 (red) and GLAP3-CSPP-L (green) and co-stained for ARL13B and CEP164 to label the TZ and the axoneme (a-ARL13B and a-CEP164, white). mCherry-CEP104 (red in cilia sketch) and GLAP3-CSPP-L (green in cilia sketch) co-localize at the tip of the primary cilium and occasionally at the axoneme (arrow in ii).

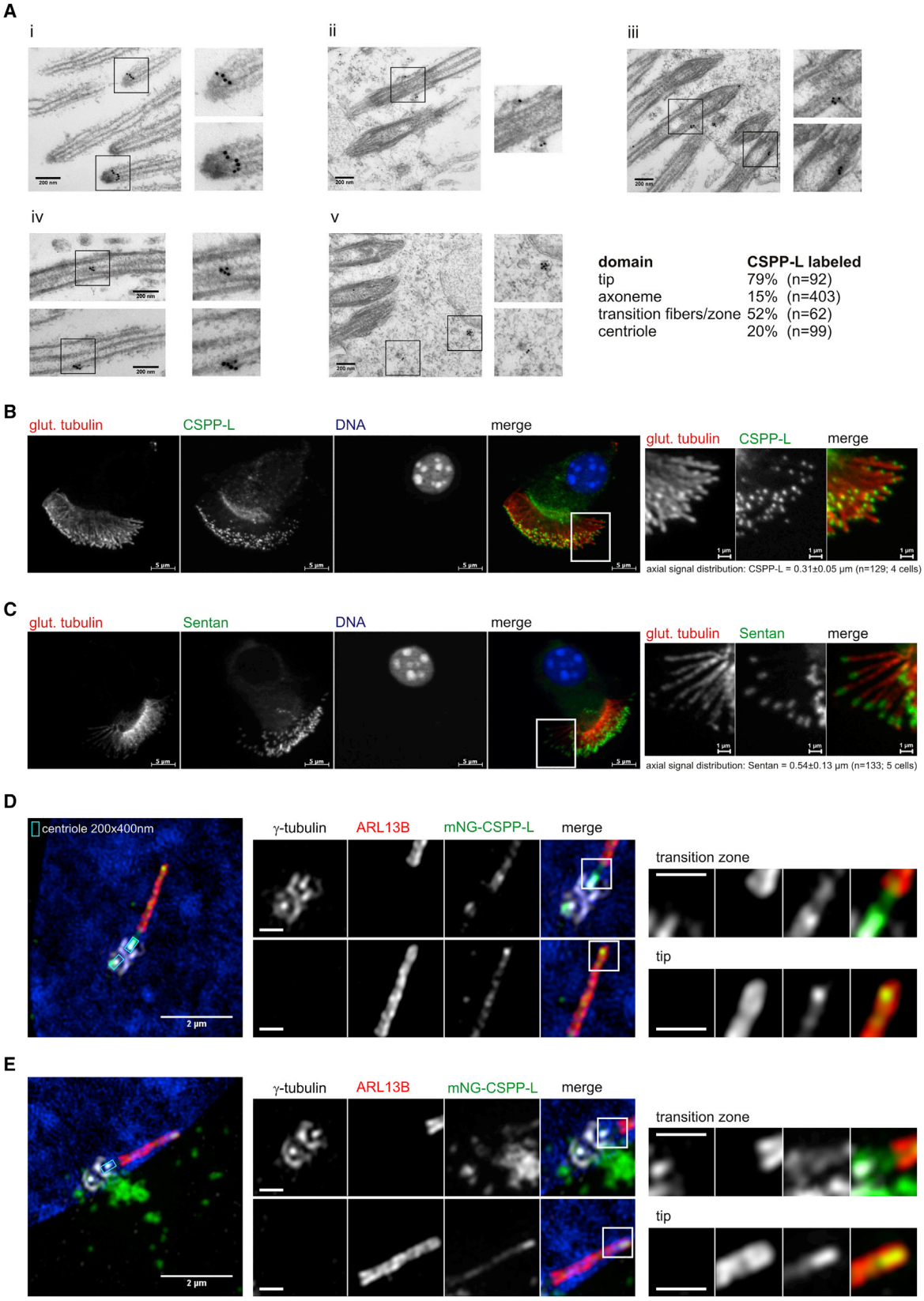

(legend on next page)

the daughter centriole (Figure 4E). Fixation conditions largely inhibit centriolar staining of glutamylated tubulin.

We conclude that interaction data, subcellular localization, and sequence analyses collectively support the notion that centrosome and cilia tip proteins CEP104 and CSPP-L interact, with a potential role in cilia axoneme MT regulation.

CSPP1 and *CEP104* Are Dispensable for Early ARL13B Recruitment but Critical for Axoneme Length Regulation

Based on the above and earlier reports on the requirement of CSPP-L and CEP104 for cilia formation (Patzke et al., 2010; Jiang et al., 2012; Satish Tammana et al., 2013), we speculated that CEP104 and CSPP-L cooperate in cilia axoneme formation. We therefore targeted *CSPP1* and *CEP104* in hTERT-RPE1 cells using CRISPR-Cas9 nickase (Ran et al., 2013). Guide RNAs (gRNAs) were designed to target *CSPP1* at the first common exon of CSPP and CSPP-L splice isoforms (Figures S5A–S5C) and *CEP104* within exon 2, just after the translational start codon (Figures S5D–S5F). Individual clones devoid of the expression of full-length CSPP-L (Figure 5A) or CEP104 (Figure 5B), respectively, were identified and characterized.

The CSPP-L-deficient clone was determined to be a compound heterozygote by allele-specific sequencing of the gRNA-targeted region. Introduced insertions putatively encode for C-terminally truncated CSPP-L proteins p.Arg267Lysfs*6 and p.Asp274Glufs*33 (Figure S5; Table S2). The expression of these or other putatively truncated CSPP1 proteins was, however, not detectable in total cell lysates using antibodies targeting the N- or C-terminal region of CSPP-L (Figure 5A); this clone is hereafter referred to as *CSPP1*$^{-/-}$ hTERT-RPE1. Likewise, a compound heterozygous *CEP104* mutant clone was identified, predicted to encode for very short mutant CEP104 proteins: p.Val10* and p.Gly13Alafs*24 (Figure S5; Table S2), respectively. However, immunoblotting using a polyclonal antibody raised against aa 201–421 of CEP104 (Jiang et al., 2012) detected two bands in a total cell lysate of this clone—a faint band at approximately 100 kDa and a more prominent band at 81 kDa, both displaying a strong reduction in expression compared to CEP104 levels in the parental hTERT-RPE1 wild-type (WT) cells (Figure 5B). Further sequence analysis identified three alternative translational start regions 3′ of the gRNA target region (Pedersen and Nielsen, 1997), promoting expression of the N-terminal truncated CEP104 proteins of 102 (Met25[360AUG]), 99 (Met50[432AUG]), and 81 kDa (Met204[969AUG]), respectively. These alternative open reading frames (ORFs) match the observed CEP104 bands. The dominantly expressed N-terminal truncated 81 kDa CEP104 protein did not co-precipitate with the CSPP-L C-terminal 379 aa domain (Figure 5C). This compound heterozygous and hypomorphic *CEP104* clone is referred to as *CEP104mut*. The generated *CSPP1*$^{-/-}$ mutant is highly reminiscent of reported homozygous and compound heterozygous *CSPP1* mutations in JBTS patients (Table S2; Figures S5A and S5D). All three reported *CEP104* JBTS-associated mutations are gene disrupting and should abrogate functional interaction with CSPP1 proteins (Table S2). Of note, the c.496C > T patient allele is likely to promote the expression of the N-terminally truncated 81 kDa CEP104 protein (Srour et al., 2015).

We next compared WT, *CSPP1*$^{-/-}$, and *CEP104mut* cells in cell-cycle progression assays, response to serum starvation, and cilia formation capability (Figures 5D and S6). A total of 69% ± 5% of WT hTERT-RPE1 cells generated a cilium upon serum withdrawal, while only 32% ± 8% of *CSPP1*$^{-/-}$ and 48% ± 9% of *CEP104mut* cells developed cilia (Figure 5D). No significant differences in cell-cycle progression were evident between asynchronously growing mutant and WT hTERT-RPE1 cells, and all three cell lines arrested in G_0/G_1 phase in response to 48 h of serum starvation (Figures S6A and S6B). Furthermore, hTERT-RPE1 mutants and WT cells showed an indistinguishable IFM pattern of acetylated tubulin, α-tubulin, and EB3 (Figures S4F and S4G). These results excluded cell-cycle progression defects and gross alterations in cytoplasmic MT organization as possible causes for defective ciliogenesis. Notably, ∼40% of *CSPP1*$^{-/-}$ and *CEP104mut* cells that failed axoneme formation (glutamylated tubulin) depicted the loss of CP110 from the mother centriole (Figure 5E; similar results obtained with CEP97, data not shown) and ∼20% recruited ARL13B to the pre-ciliary vesicle (Figure 5F), indicating that cilia formation was impaired at an axoneme-forming permissive stage. Axoneme length in *CSPP1*$^{-/-}$ (1.5 ± 0.05 μm) and *CEP104mut* (1.9 ± 0.06 μm) cells was significantly reduced compared to WT cells (2.9 ± 0.05 μm) (Figure 5G), suggesting a cilia-specific defect in MT organization. Cilia length was rescued in *CSPP1*$^{-/-}$ cells by mNG-CSPP-L (Figure S6E). In contrast to *cep104* rescue experiments in zebrafish, the expression of mNG-CEP104 in *CEP104mut* cells did not rescue the cilia phenotype at statistical significance. This is likely due to a dominant negative effect of the N-terminally truncated CEP104 proteins expressed in these cells (Figures 5B and S6F). The antagonizing effects of EF1α-promotor-driven NeonGreen fusion proteins cannot be excluded as both fusion proteins are overexpressed compared to endogenous levels. Nonetheless, IFM analysis of mNG-CSPP-L expressing *CEP104mut* and mNG-CEP104 expressing *CSPP1*$^{-/-}$ cells revealed ciliary localization for both proteins (Figures 5H, 5I, S6E, and S6F). Hence, intra-ciliary interaction of CEP104-CSPP-L is required to achieve regular axoneme length.

Figure 3. Ciliary Localization of CSPP-L at Motile and Primary Cilia

(A) CSPP-L detection by post-embedding IEM of mouse tracheal epithelial cells. Panels depict close ups of (i) cilia tips, (ii and iii) basal bodies, (iv) cilia axonemes, and (v) apically localized electron-dense particles.

(B and C) IFM of mouse tracheal epithelial cells showing axonemal MTs (glutamylated tubulin, red) and CSPP-L (B, green) or Sentan (C, green). Right panels show magnifications of indicated regions.

(D and E) 3D-SIM IFM of hTERT-RPE1 cells expressing monomeric NeonGreen (mNG)-CSPP-L and co-stained for centrosomal marker γ-tubulin (white) and cilia membrane marker ARL13B (red). Scale bars in magnified areas, 500 nm.

mNG-CSPP-L decorates axonemal MTs throughout the transition zone and concentrates at the tip (D and E). Centriolar satellite localization is frequently found and exemplified in (E) and Figure S4C.

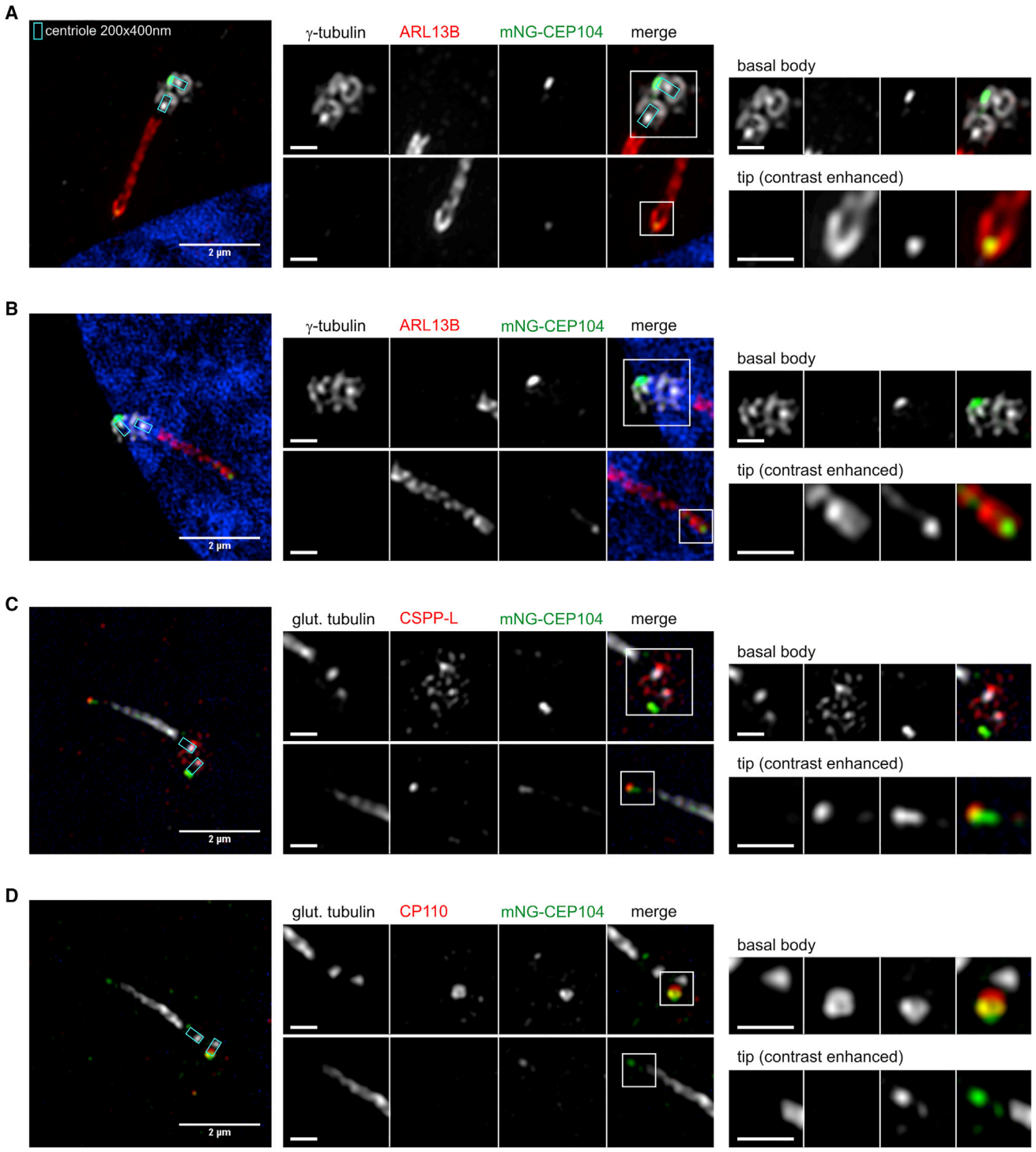

Figure 4. Localization of mNG-CEP104 and CSPP-L at Primary Cilia

(A–D) 3D-SIM IFM of hTERT-RPE1 cells expressing mNG-CEP104 (green) and co-stained for centrosomal marker γ-tubulin (white) and cilia membrane marker ARL13B (red). (A and B) Glutamylated tubulin (white) and CSPP-L (red) (C) or glutamylated tubulin (white) and CP110 (red) (D). Scale bars in magnified areas, 500 nm. mNG-CEP104 localizes to the capping complex of the daughter centriole (A, B, and D) and co-localizes with CSPP-L at the cilia tip (C). Low cilia tip signal intensity of mNG-CEP104 compared to daughter centriole localization is observed in all of the cells. Axoneme staining of CSPP-L is fixation condition dependent (Patzke et al., 2010; Hua and Ferland, 2017) and not resolved.

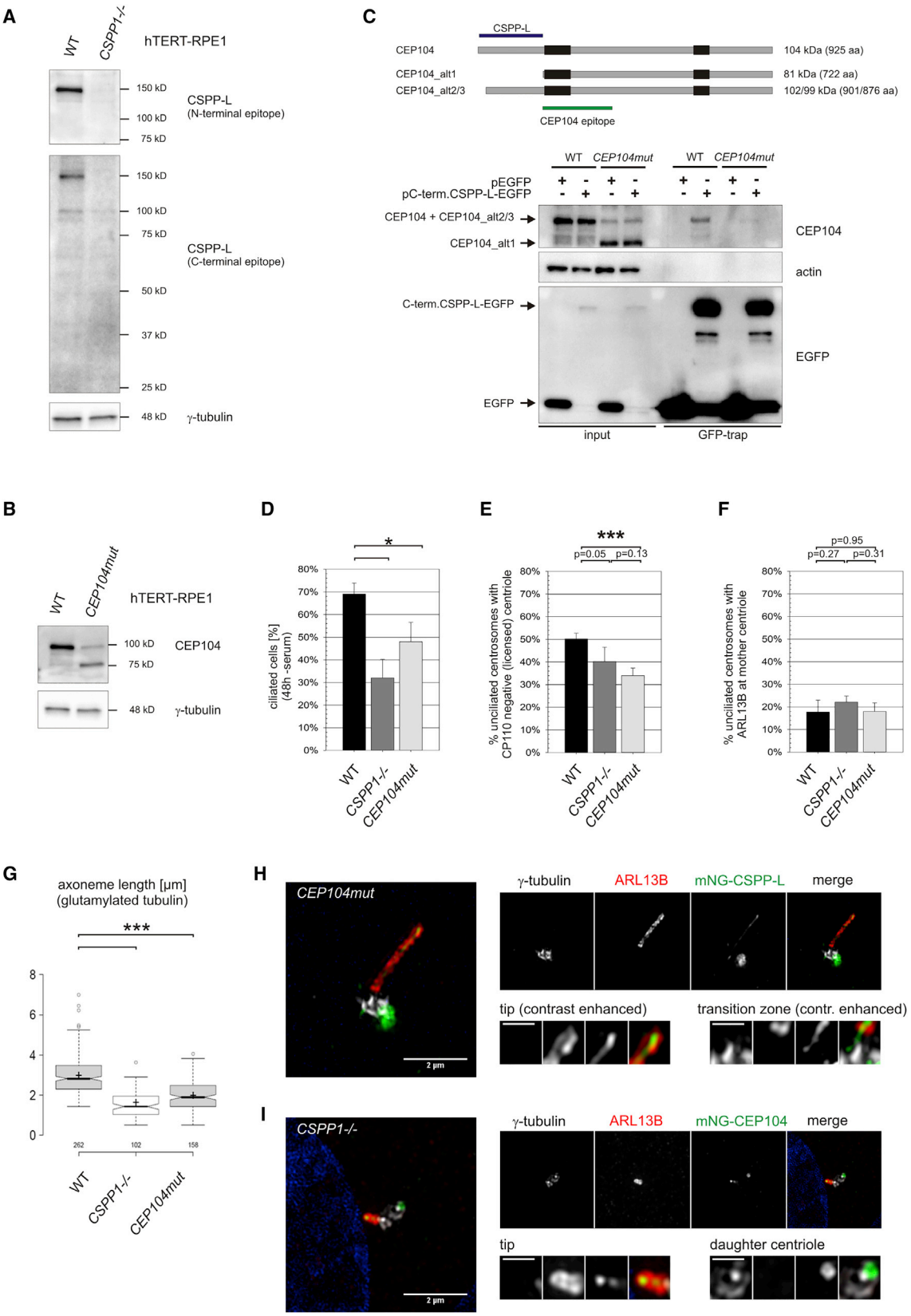

(legend on next page)

Depletion of CEP104 in *CSPP1*$^{-/-}$ cells strongly diminished cilia formation (Figure S6G), further supporting this hypothesis.

These data suggest that neither *CEP104* nor *CSPP1* are strictly essential for the initial stages of cilia formation but that their intra-ciliary interaction is critical for regular axoneme elongation or maintenance.

CSPP1$^{-/-}$ and *CEP104mut* Cilia Are Defective in SMO Translocation in Response to Hh Pathway Activation

The cilia phenotypes in *CSPP1*$^{-/-}$ and *CEP104mut* cells are in agreement with reported cilia aberrations in *CSPP1* and *CEP104* mRNA targeting small interfering RNA (siRNA) transfectants (Patzke et al., 2010; Jiang et al., 2012; Satish Tammana et al., 2013). In contrast to *CSPP1*, a cilia phenotype in *CEP104* mutated JBTS patients has not yet been reported. *CSPP1*-mutated JBTS patient fibroblasts are deficient in SHH-induced GLI1 expression, as determined by bulk analysis (Tuz et al., 2014; Shaheen et al., 2014). To discriminate whether the reported SHH sensitivity defect could be attributed to reduced cilia numbers or defective cilia function and whether *CEP104mut* cells share pathway impairment, we investigated the efficacy of Smoothened (SMO) translocation to cilia in response to Hh pathway activation by soluble SHH-ligand (ShhN) conditioned medium or 100 nM Smoothened agonist (SAG) treatment (Figure 6). Cells were serum starved for 48 h to promote cilia formation and then stimulated for 24 h before fixation and assessment of SMO and ARL13B by IFM. Semiquantitative assessment revealed that *CSPP1*$^{-/-}$ and particularly *CEP104mut* cells had significantly decreased SMO translocation to primary cilia in response to ShhN stimulation compared to WT hTERT-RPE1 cells (Figure 6A). Similarly, the quantitative assessment of median ciliary fluorescence intensities of ARL13B and SMO in SAG-treated cells revealed a strong dependence of ciliary SMO accumulation on *CEP104* (30% of WT SMO intensity) and to a lesser extent on *CSPP1* (70% of WT SMO intensity) integrity (Figure 6B). In contrast, median ciliary ARL13B intensities were indistinguishable between cell lines. Likewise, cilia membrane localization of the ARL13B-dependent Hh pathway modulator INPP5E (Figure 6C) (Humbert et al., 2012; Garcia-Gonzalo et al., 2015; Chávez et al., 2015) and the ARL13B regulatory TZ proteins CBY1 (Figure S6J) and AHI1 (Figure S6K) (Lee et al., 2014) were not decreased in *CSPP1*$^{-/-}$ or *CEP104mut* cells. Finally, the localization pattern of IFT88 indicated *CEP104* and *CSPP1* independent ciliary entry and tip localization of the IFT-B core complex (Figure S6L).

We conclude that the cilia tip protein CEP104 is a critical factor for Hh signaling in hTERT-RPE1 cells. These data support the hypothesis that defective ciliary Hh signaling causes the perturbed heart and cranial nerve development observed in *cep104* morphant zebrafish embryos.

DISCUSSION

The disturbance of physical interaction networks between proteins encoded by disease genes of a distinct ciliopathy is likely to explain the observed genetic heterogeneity and account for certain genetic overlap between phenotypically related ciliopathies, such as JBTS, NPHP, MKS, or BBS (Sang et al., 2011; Nachury et al., 2007). In the case of JBTS, 35 disease loci have been identified to date; almost all of the affected proteins are exclusively connected to the TZ and the regulation of Hh signaling. *CEP104* is an exception to this understanding, by (1) being localized to the daughter centriole and the ciliary tip, but not the mother centriole or the TZ of the cilium and/or basal body entity (Jiang et al., 2012; Satish Tammana et al., 2013), and (2) having an undetermined role in Hh signaling or interaction with other JBTS proteins. The identified interaction with CSPP-L (Figure 2) and the *cep104* zebrafish ciliopathy phenotypes (Figures 1 and S7) reported here resolve this apparent discrepancy and, in context with reported mutations in *KIF7* (alias *JBTS12*) and *KIAA0556* (alias *JBTS26*), contribute evidence to the expansion of the JBTS network to the ciliary tip compartment (Dafinger et al., 2011; He et al., 2014; Sanders et al., 2015).

The combined interaction data and cilia analysis in *CEP104mut* and *CSPP1*$^{-/-}$ cells identify a requirement for CEP104/CSPP-L interplay to form Hh signaling-competent cilia (Figure 7). Mutual independence for ciliary localization and the severe ciliation deficiency phenotype in co-depleted cells suggest that the intra-ciliary interaction of CSPP-L with CEP104 is essential for attaining normal cilia stature. The inhibition of ciliogenesis after CP110/CEP97 release and the formation of shortened, ARL13B-positive cilia in *CSPP1*$^{-/-}$ cells are in concordance with reported phenotypes in *CSPP1* JBTS patient fibroblasts (Akizu et al., 2014; Shaheen et al., 2014; Tuz et al., 2014; Figures 1 and 5) and imply that CSPP-L is not strictly required for cilium formation until axoneme elongation.

Figure 5. Intra-ciliary Interaction of CEP104 and CSPP-L Is Critical for Axoneme Length

(A) *CSPP1*$^{-/-}$ hTERT-RPE1 cells are negative for the expression of CSPP-L full-length or truncated CSPP1 proteins, as determined by immunoblotting with N-terminal and C-terminal domain-specific CSPP-L antibodies and compared to γ-tubulin (loading control).

(B and C) *CEP104mut* hTERT-RPE1 cells express N-terminally truncated CEP104 proteins at strongly decreased expression levels compared to WT hTERT-RPE1 cells by use of alternative start codons (B). The prominent truncated CEP104 protein of 81 kDa, lacking the N-terminal 203 aa does not co-purify with the C-terminal CSPP-L domain expressed in hTERT-RPE1 transfectants (C).

(D) *CSPP1*$^{-/-}$ and *CEP104mut* hTERT-RPE1 cells form primary cilia at lower frequency (error bars depict SEM of 3 experiments; n = 150 cells; t test; *$p < 0.05$).

(E and F) A total of 40% of *CSPP1*$^{-/-}$ and 34% of *CEP104mut* hTERT-RPE1 cells without detectable glutamylated axoneme have licensed mother centrioles (i.e., single CP110 signal) compared to 50% in WT hTERT-RPE1 cells (E). Independent of genotype, ~20% of non-ciliated cells show ARL13B signal at the mother centriole, indicative of pre-ciliary vesicle formation (F). Error bars depict SEM of 4 experiments (n = 150 cells; t test; ***$p < 0.005$).

(G) Cilia in *CSPP1*$^{-/-}$ and *CEP104mut* hTERT-RPE1 cells have decreased axoneme length (center lines in boxplots show the medians; box limits indicate the 25th and 75th percentiles as determined by R software; whiskers extend 1.5 times the interquartile range from the 25th and 75th percentiles; outliers are represented by dots; crosses represent sample means; n = 262, 102, 158 sample points; t test; ***$p < 0.005$).

(H and I) 3D-SIM IFM of *CEP104mut* hTERT-RPE1 cells stably expressing mNG-CSPP-L (H) and *CSPP1*$^{-/-}$ hTERT-RPE1 cells stably expressing mNG-CEP104 (I). mNG-CSPP-L and mNG-CEP104 show no gross localization defects to primary cilia (ARL13B, red) or the centrosome (γ-tubulin, white).

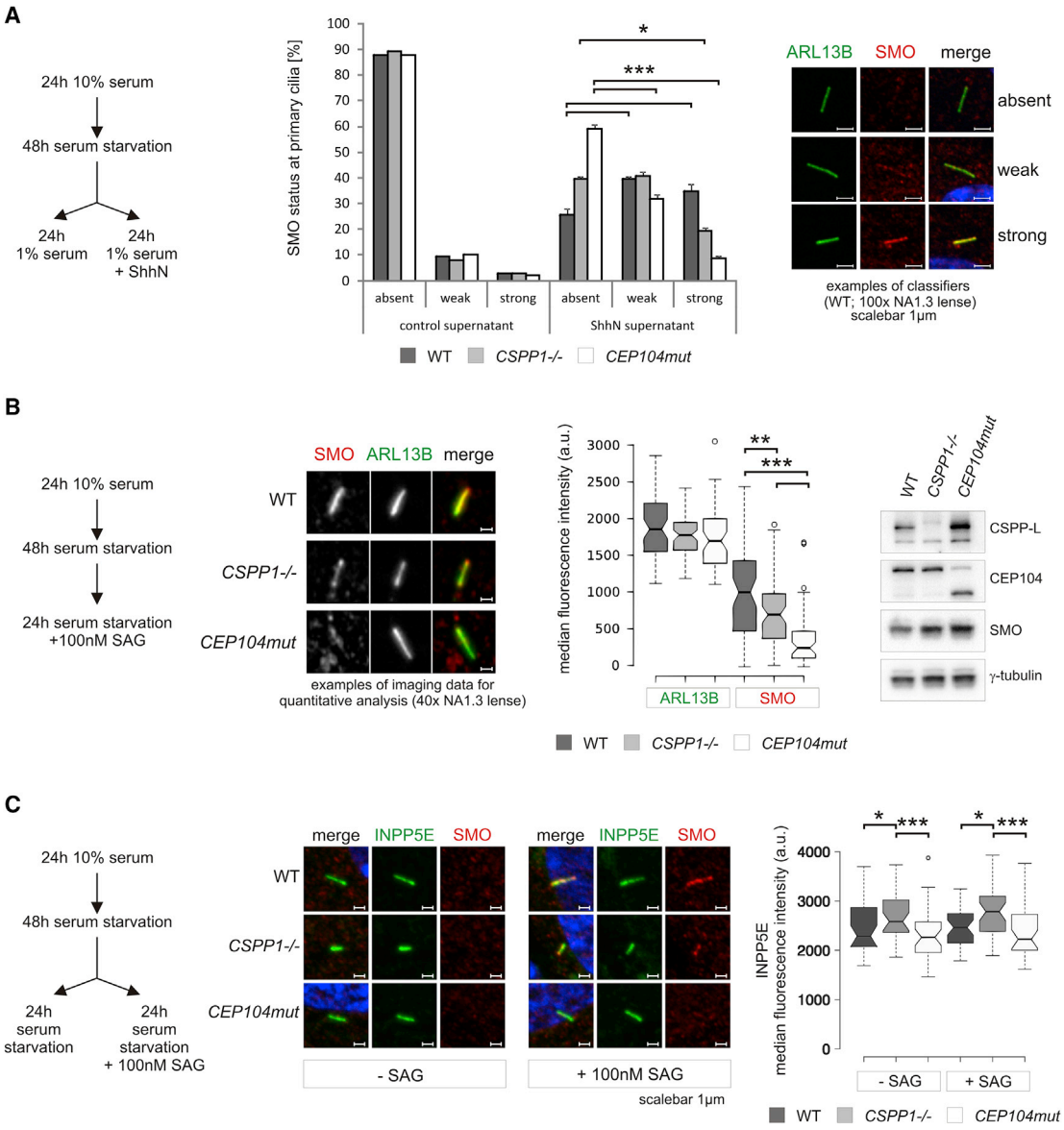

Figure 6. Deficient Ciliary SMO Accumulation in *CEP104mut* and *CSPP1*$^{-/-}$ hTERT-RPE1 Cells in Response to Hh Pathway Activation

(A) Assessment of ciliary SMO translocation in response to Hh signaling pathway stimulation by addition of ShhN conditioned medium. Cells were serum starved for 48 h in 2 mL DMEM/F12 before replacement of 1 mL with ShhN conditioned or control DMEM containing 2% serum and further incubation for 24 h. *CSPP1*$^{-/-}$ and *CEP104mut* hTERT-RPE1 show decreased SMO (a-SMO; red) accumulation to the primary cilium (a-ARL13B, green). Ciliary SMO levels were scored by inspection and classified in absent, weak, or strong subgroups. Error bars in bar graph depict SEMs of 3 independent experiments, n = 150 per treatment and cell line; t test; *$p < 0.05$ and ***$p < 0.001$).

(B) Quantitative assessment of median fluorescence intensities of ciliary ARL13B (a-ARL13B, green) and SMO (a-SMO, red) in serum-starved and SAG-stimulated WT (n = 60), *CSPP1*$^{-/-}$ (n = 66), and *CEP104mut* (n = 52) hTERT-RPE1 cells (t test; **$p < 0.01$ and ***$p < 0.001$), and determination of SMO expression in total cell lysates of SAG-treated cell lines by immunoblotting.

(C) Quantitative assessment of ciliary INPP5E by IFM in SAG-stimulated and non-stimulated serum-starved WT, *CSPP1*$^{-/-}$, and *CEP104mut* hTERT-RPE1 cells (a-INPP5E, green; a-SMO, red) (n > 30 in each treatment group; t test; *$p < 0.05$ and ***$p \leq 0.001$).

Center lines in boxplots show the medians; box limits indicate the 25th and 75th percentiles as determined by R software; whiskers extend 1.5 times the interquartile range from the 25th and 75th percentiles; outliers are represented by dots. Scale bars, 1 µm.

CEP104 binds via its N-terminal domain to the C-terminal domain of CSPP-L, which is dispensable for the localization of CSPP-L to MTs but critical for the regulation of the effect of CSPP-L on MT organization (Patzke et al., 2006, 2010). In analogy to CEP97-mediated CEP104 localization to cytoplasmic MT plus ends (Jiang et al., 2012), CEP104 and CSPP-L may mutually enhance MT stabilization at the ciliary tip compartment. CSPP-L-dependent CEP104 stabilization at the axoneme lattice

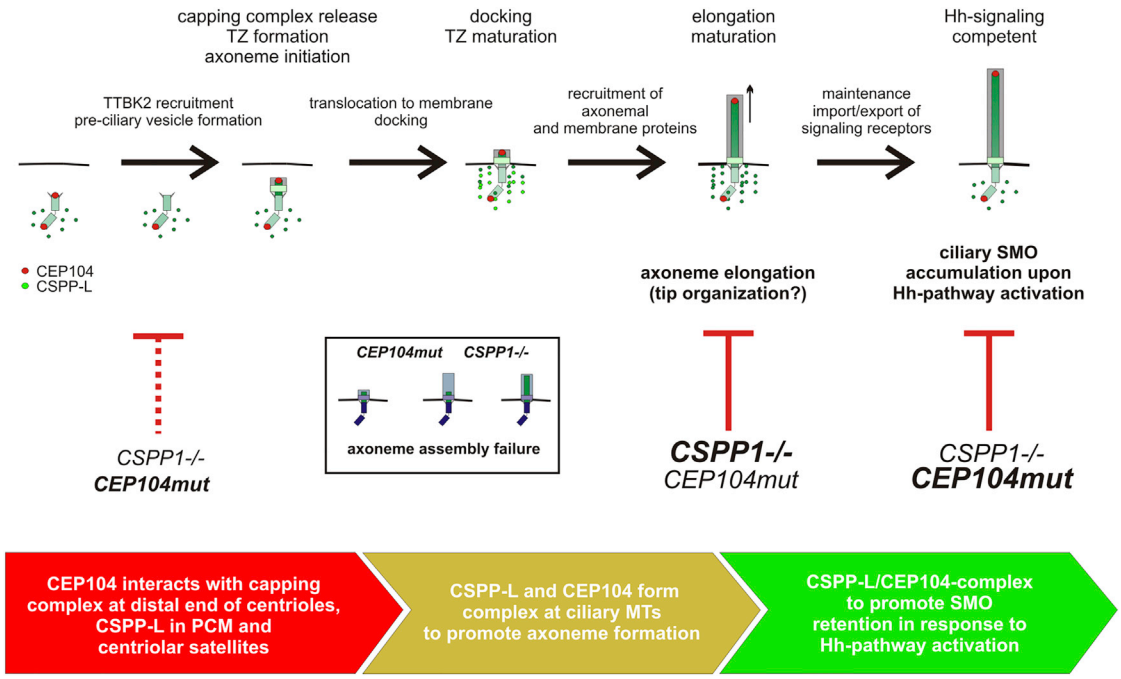

Figure 7. Graphical Summary of CEP104 and CSPP-L Interplay for Formation of Hh Signaling Pathway-Competent Primary Cilia

in the tip region could enhance CEP104-mediated tubulin addition at MT plus ends, as suggested by Al-Jassar et al. (2017) and supported by the severe ciliation defect of CEP104 in depleted *CSPP1*$^{-/-}$ cells. Speculatively, the CSPP-L/CEP104 complex hence opposes KIF7 and KIAA0556 mediated axoneme growth restriction at the ciliary tip (He et al., 2014; Sanders et al., 2015). Future studies are warranted, including advanced *in vitro* and live cell imaging analyses, to determine the detailed effect of CSPP-L/CEP104 complexes on isolated MTs and to elucidate their potential dynamic behavior during cilia formation and maintenance.

The positive role of CEP104 in cilia formation and requirement for ciliary SMO accumulation in hTERT-RPE1 cells resembles the requirement of cep104 *in vivo*, in which shortened cilia in Kupffer's vesicle of *cep104* morphant and crispant zebrafish embryos were observed. Ciliary morphology was regained by co-administration of human *CEP104* mRNA (Figures 1 and S2). Likewise, the loss of cep104 manifested in the mal-development of the heart and the cranial nerves, the latter being highly reminiscent of the defective development of the mid- and/or hindbrain characteristic of JBTS. Accumulating evidence supports the hypothesis that defective ciliary Hh signaling is the underlying cause of the phenotype associated with JBTS (Hynes et al., 2014; Roosing et al., 2015; Aguilar et al., 2012). Bulk analysis of *CSPP1* JBTS patient fibroblasts showed reduced Hh signaling pathway activity sensitivity and/or responsiveness (reduced Hh-induced *GLI1* mRNA expression [Shaheen et al., 2014]). Cardiac developmental defects in *cep104* zebrafish morphants may be a consequence of laterality defects. Lost Shh sensitivity may have a contributing effect, since highly similar ventricle size and orientation defects are seen in smo-deficient or cyclopamine-treated (an Hh antagonist) embryos (Thomas et al., 2008). A role for cilia in cardiac development is well established (Li et al., 2015). Congenital heart defects are evident in JBTS and NPHP patients (Koefoed et al., 2014; San Agustin et al., 2016), but they are not reported for rare *CEP104*-mutated JBTS patients (Srour et al., 2015). Comparable to our loss-of-function studies, these three *CEP104* patients carry either nonsense or splice-site mutations. However, it is known that dependent on the JBTS model system, Hh signaling may be increased, as shown in *CEP290* patient fibroblasts (Shimada et al., 2017), or decreased, as in murine models of Cep290 knockdown (Hynes et al., 2014). It cannot be excluded that other *CEP104* mutations, including gain-of-function mutations, may cause embryonic lethality in humans, but *CEP104* mutations have not been observed in MKS embryos thus far.

Functional analysis of our hTERT-RPE1 cell lines determined that CSPP-L and, in particular, CEP104 mutant cilia are Hh pathway compromised in a manner that is distinct from the ciliary INPP5E regulating pathway found targeted in JBTS (Humbert et al., 2012; Bielas et al., 2009; Jacoby et al., 2009; Thomas et al., 2014; Cantagrel et al., 2008; Ferland et al., 2004; Slaats et al., 2016). Our analysis of ShhN or SAG-induced SMO translocation to the cilia compartment revealed a significantly stronger impairment in *CEP104mut* than in *CSPP1*$^{-/-}$ cells (Figure 6), suggesting that CSPP-L may potentiate the capability of CEP104 at the tip compartment in regulating ciliary SMO turnover in response to Hh pathway stimulation. This is different from *PDE6D*, *ARL13B*, and *INPP5E* compromising JBTS-related mutants, which recruit SMO (Humbert et al., 2012; Garcia-Gonzalo et al., 2015; Chávez et al., 2015; Larkins et al., 2011). Of note, Tuz et al. (2014) observed reduced ciliary ARL13B levels in *CSPP1* JBTS patient fibroblasts. This is not recapitulated

in our quantitative analysis of ARL13B and INPP5E in hTERT-RPE1 cells (Figure 6) and may thus be either cell type dependent or mutation specific. 3D-SIM revealed that mNG-CSPP-L extends from the central lumen of the mother centriole into the cilia compartment (Figures 3D and 3E), a localization pattern that is partially supported by fixation/antibody-dependent immunoelectron microscopy (immuno-EM) (Figure 3A) and IFM (Patzke et al., 2010; Hua and Ferland, 2017). We and others have shown previously that CSPP-L is required for the localization of the larger retinitis pigmentosa guanosine triphophatase (GTPase) regulator-interacting protein 1-like (RPGRIP1-LIKE) at the TZ (Patzke et al., 2010; Shaheen et al., 2014), which is an Hh signaling pathway modulator in mouse embryonic fibroblasts (Vierkotten et al., 2007). A contribution of a TZ defect to the reduced SMO translocation phenotype can thus not be fully excluded in *CSPP1*$^{-/-}$ hTERT-RPE1 cells. In contrast, CSPP-L is present at the cilia of *CEP104mut* hTERT-RPE1 cells, which is unlikely to bear a TZ defect.

Inferring from the flagellar defects in the FAP256 mutants in *Chlamydomonas* (Satish Tammana et al., 2013) and *Tetrahymena* (Louka et al., 2018), structural aberrations at the tip of the primary cilia of *CEP104mut* cells are likely to be expected. However, *KIF7*$^{-/-}$ mouse embryonic fibroblasts (MEFs) do gain ciliary SMO in response to Hh pathway stimulation (He et al., 2014), suggesting that structural defects at the cilia tip may not affect the ciliary accumulation of SMO per se. Peripheral IFT-B sub-complex IFT25/IFT27 defective MEFs show a complementary phenotype and accumulate SMO in cilia, even in the absence of pathway stimulation, indicating SMO regulation at the export level (Eguether et al., 2014; Keady et al., 2012). Under the presumption of a similar balance existing in hTERT-RPE1 cells, ciliary export of SMO may be favored in Hh-unstimulated WT, *CEP104mut*, and likely also *CSPP1*$^{-/-}$ hTERT-RPE1 cells. One may hypothesize that CEP104, beyond its architectural function, could interfere via its IFT25-homologous N-terminal domain with IFT25/IFT27 at the cilia tip to regulate ciliary residence of SMO in response to pathway activation (Keady et al., 2012; Eguether et al., 2014; Huet et al., 2014; Bhogaraju et al., 2011; Milenkovic et al., 2015). In support of this idea, we have detected an interaction between recombinant CEP104 and IFT27 in preliminary experiments (Figure S7), but the validation and functional analyses warrant a study in their own right.

To conclude, we demonstrate *in vitro* and *in vivo* that ciliary complex formation of CEP104 and CSPP-L is essential for Hh signal-competent tip compartment and/or axoneme formation, indicating abrogation of this process as the underlying molecular defect in JBTS resulting from *CEP104* mutations. The localization pattern of CSPP-L defines an interesting link between the centriolar satellite and the MT axoneme compartment. Further investigations on the dynamic regulation of cilia tip and centriolar satellite protein networks may thus provide a future avenue of ciliopathy research.

STAR★METHODS

Detailed methods are provided in the online version of this paper and include the following:

SUPPLEMENTAL INFORMATION

Supplemental Information can be found online at https://doi.org/10.1016/j.celrep.2019.07.025.

ACKNOWLEDGMENTS

We are thankful to Kristen J. Verhey (University of Michigan, Ann Arbor, MI, USA), Esben Lorentzen (Aarhus University, Aarhus, Denmark), Bradley K. Yoder (Department of Cell Biology, University of Alabama, Birmingham, AL, USA), and Akiharu Kubo (Keio University, Tokyo, Japan) for providing reagents. S.P. is funded by a career development fellowship from the Norwegian Cancer Society (6839316). J.A.S. is funded by the Northern Counties Kidney Research Fund, Kidney Research UK, and the Medical Research Council (MR/M012212/1). S.A.R. is a Kidney Research UK fellow. E.M. is funded by Kids Kidney Research and Kidney Research UK. R.H.G. and R.R. acknowledge funding from the European Union (EU) FP7 program "SYSCILIA" (no. 241955) and the Dutch Kidney Foundation "KOUNCIL" Consortium (CP11.18). R.R. is funded by the Netherlands Organization for Scientific Research (NWO Vici-865.12.005). L.B.P. acknowledges funding from the Novo Nordisk Foundation (NNF15OC0016886 and NNF18OC0053024), the Danish Cancer Society (R146-A9590-16-S2), the Independent Research Fund Denmark (8020-00162B), and the Carlsberg Foundation (CF18-0294).

AUTHOR CONTRIBUTIONS

Conceptualization, J.A.S. and S.P.; Methodology, A.A., R.R., T.S., S.G., L.B.P., K.O.S., J.A.S., and S.P.; Formal Analysis, K.-A.M.F., M.T., J.A.S., and S.P.; Investigation, K.-A.M.F., M.T., S.A.R., E.M., F.H., S.G., K.O.S., S.J.F.L., R.H.G., R.R., J.A.S., and S.P.; Writing—Original Draft, J.A.S. and S.P.; Writing—Review and Editing, K.-A.M.F., R.H.G., A.A., R.R., T.S., S.A.R., E.M., J.A.S., L.B.P., and S.P.; Funding Acquisition, J.A.S. and S.P.; Resources, A.A. and R.R.; Supervision, J.A.S. and S.P.

DECLARATION OF INTERESTS

The authors declare no competing interests.

Received: July 26, 2017
Revised: May 21, 2019
Accepted: July 10, 2019
Published: August 13, 2019

REFERENCES

Aguilar, A., Meunier, A., Strehl, L., Martinovic, J., Bonniere, M., Attie-Bitach, T., Encha-Razavi, F., and Spassky, N. (2012). Analysis of human samples reveals impaired SHH-dependent cerebellar development in Joubert syndrome/Meckel syndrome. Proc. Natl. Acad. Sci. USA *109*, 16951–16956.

Akhmanova, A., and Steinmetz, M.O. (2015). Control of microtubule organization and dynamics: two ends in the limelight. Nat. Rev. Mol. Cell Biol. *16*, 711–726.

Akizu, N., Silhavy, J.L., Rosti, R.O., Scott, E., Fenstermaker, A.G., Schroth, J., Zaki, M.S., Sanchez, H., Gupta, N., Kabra, M., et al. (2014). Mutations in CSPP1 lead to classical Joubert syndrome. Am. J. Hum. Genet. *94*, 80–86.

Al-Bassam, J., and Chang, F. (2011). Regulation of microtubule dynamics by TOG-domain proteins XMAP215/Dis1 and CLASP. Trends Cell Biol. *21*, 604–614.

Al-Jassar, C., Andreeva, A., Barnabas, D.D., McLaughlin, S.H., Johnson, C.M., Yu, M., and van Breugel, M. (2017). The Ciliopathy-Associated Cep104 Protein Interacts with Tubulin and Nek1 Kinase. Structure *25*, 146–156.

Bangs, F., and Anderson, K.V. (2017). Primary Cilia and Mammalian Hedgehog Signaling. Cold Spring Harb. Perspect. Biol. *9*, a028175.

Bhogaraju, S., Taschner, M., Morawetz, M., Basquin, C., and Lorentzen, E. (2011). Crystal structure of the intraflagellar transport complex 25/27. EMBO J. *30*, 1907–1918.

Bhogaraju, S., Cajanek, L., Fort, C., Blisnick, T., Weber, K., Taschner, M., Mizuno, N., Lamla, S., Bastin, P., Nigg, E.A., and Lorentzen, E. (2013). Molecular basis of tubulin transport within the cilium by IFT74 and IFT81. Science *341*, 1009–1012.

Bielas, S.L., Silhavy, J.L., Brancati, F., Kisseleva, M.V., Al-Gazali, L., Sztriha, L., Bayoumi, R.A., Zaki, M.S., Abdel-Aleem, A., Rosti, R.O., et al. (2009). Mutations in INPP5E, encoding inositol polyphosphate-5-phosphatase E, link phosphatidyl inositol signaling to the ciliopathies. Nat. Genet. *41*, 1032–1036.

Campeau, E., Ruhl, V.E., Rodier, F., Smith, C.L., Rahmberg, B.L., Fuss, J.O., Campisi, J., Yaswen, P., Cooper, P.K., and Kaufman, P.D. (2009). A versatile viral system for expression and depletion of proteins in mammalian cells. PLoS One *4*, e6529.

Cantagrel, V., Silhavy, J.L., Bielas, S.L., Swistun, D., Marsh, S.E., Bertrand, J.Y., Audollent, S., Attié-Bitach, T., Holden, K.R., Dobyns, W.B., et al.; International Joubert Syndrome Related Disorders Study Group (2008). Mutations in the cilia gene ARL13B lead to the classical form of Joubert syndrome. Am. J. Hum. Genet. *83*, 170–179.

Chávez, M., Ena, S., Van Sande, J., de Kerchove d'Exaerde, A., Schurmans, S., and Schiffmann, S.N. (2015). Modulation of Ciliary Phosphoinositide Content Regulates Trafficking and Sonic Hedgehog Signaling Output. Dev. Cell *34*, 338–350.

Chih, B., Liu, P., Chinn, Y., Chalouni, C., Komuves, L.G., Hass, P.E., Sandoval, W., and Peterson, A.S. (2011). A ciliopathy complex at the transition zone protects the cilia as a privileged membrane domain. Nat. Cell Biol. *14*, 61–72.

Christensen, S.T., Morthorst, S.K., Mogensen, J.B., and Pedersen, L.B. (2017). Primary Cilia and Coordination of Receptor Tyrosine Kinase (RTK) and Transforming Growth Factor β (TGF-β) Signaling. Cold Spring Harb. Perspect. Biol. *9*, a028167.

Dafinger, C., Liebau, M.C., Elsayed, S.M., Hellenbroich, Y., Boltshauser, E., Korenke, G.C., Fabretti, F., Janecke, A.R., Ebermann, I., Nürnberg, G., et al. (2011). Mutations in KIF7 link Joubert syndrome with Sonic Hedgehog signaling and microtubule dynamics. J. Clin. Invest. *121*, 2662–2667.

Dale Rein, I., Solberg Landsverk, K., Micci, F., Patzke, S., and Stokke, T. (2015). Replication-induced DNA damage after PARP inhibition causes G2 delay, and cell line-dependent apoptosis, necrosis and multinucleation. Cell Cycle *14*, 3248–3260.

Eguether, T., San Agustin, J.T., Keady, B.T., Jonassen, J.A., Liang, Y., Francis, R., Tobita, K., Johnson, C.A., Abdelhamed, Z.A., Lo, C.W., and Pazour, G.J. (2014). IFT27 links the BBSome to IFT for maintenance of the ciliary signaling compartment. Dev. Cell *31*, 279–290.

Ferland, R.J., Eyaid, W., Collura, R.V., Tully, L.D., Hill, R.S., Al-Nouri, D., Al-Rumayyan, A., Topcu, M., Gascon, G., Bodell, A., et al. (2004). Abnormal cerebellar development and axonal decussation due to mutations in AHI1 in Joubert syndrome. Nat. Genet. *36*, 1008–1013.

Garcia-Gonzalo, F.R., Corbit, K.C., Sirerol-Piquer, M.S., Ramaswami, G., Otto, E.A., Noriega, T.R., Seol, A.D., Robinson, J.F., Bennett, C.L., Josifova, D.J., et al. (2011). A transition zone complex regulates mammalian ciliogenesis and ciliary membrane composition. Nat. Genet. *43*, 776–784.

Garcia-Gonzalo, F.R., Phua, S.C., Roberson, E.C., Garcia, G., 3rd, Abedin, M., Schurmans, S., Inoue, T., and Reiter, J.F. (2015). Phosphoinositides Regulate Ciliary Protein Trafficking to Modulate Hedgehog Signaling. Dev. Cell *34*, 400–409.

Gupta, G.D., Coyaud, É., Gonçalves, J., Mojarad, B.A., Liu, Y., Wu, Q., Gheiratmand, L., Comartin, D., Tkach, J.M., Cheung, S.W., et al. (2015). A Dynamic Protein Interaction Landscape of the Human Centrosome-Cilium Interface. Cell *163*, 1484–1499.

Hauge, H., Patzke, S., and Aasheim, H.C. (2007). Characterization of the FAM110 gene family. Genomics *90*, 14–27.

He, M., Subramanian, R., Bangs, F., Omelchenko, T., Liem, K.F., Jr., Kapoor, T.M., and Anderson, K.V. (2014). The kinesin-4 protein Kif7 regulates mammalian Hedgehog signalling by organizing the cilium tip compartment. Nat. Cell Biol. *16*, 663–672.

Higashijima, S., Hotta, Y., and Okamoto, H. (2000). Visualization of cranial motor neurons in live transgenic zebrafish expressing green fluorescent protein under the control of the islet-1 promoter/enhancer. J. Neurosci. *20*, 206–218.

Hildebrand, A., Remmert, M., Biegert, A., and Soding, J. (2009). Fast and accurate automatic structure prediction with HHpred. Proteins *77* (*Suppl 9*), 128–132.

Hua, K., and Ferland, R.J. (2017). Fixation methods can differentially affect ciliary protein immunolabeling. Cilia *6*, 5.

Huang, C.J., Tu, C.T., Hsiao, C.D., Hsieh, F.J., and Tsai, H.J. (2003). Germ-line transmission of a myocardium-specific GFP transgene reveals critical regulatory elements in the cardiac myosin light chain 2 promoter of zebrafish. Dev. Dyn. *228*, 30–40.

Huerta-Cepas, J., Szklarczyk, D., Forslund, K., Cook, H., Heller, D., Walter, M.C., Rattei, T., Mende, D.R., Sunagawa, S., Kuhn, M., et al. (2016). eggNOG 4.5: a hierarchical orthology framework with improved functional annotations for eukaryotic, prokaryotic and viral sequences. Nucleic Acids Res. *44*, D286–D293.

Huet, D., Blisnick, T., Perrot, S., and Bastin, P. (2014). The GTPase IFT27 is involved in both anterograde and retrograde intraflagellar transport. Elife *3*, e02419.

Humbert, M.C., Weihbrecht, K., Searby, C.C., Li, Y., Pope, R.M., Sheffield, V.C., and Seo, S. (2012). ARL13B, PDE6D, and CEP164 form a functional network for INPP5E ciliary targeting. Proc. Natl. Acad. Sci. USA *109*, 19691–19696.

Hynes, A.M., Giles, R.H., Srivastava, S., Eley, L., Whitehead, J., Danilenko, M., Raman, S., Slaats, G.G., Colville, J.G., Ajzenberg, H., et al. (2014). Murine Joubert syndrome reveals Hedgehog signaling defects as a potential therapeutic target for nephronophthisis. Proc. Natl. Acad. Sci. USA *111*, 9893–9898.

Jacoby, M., Cox, J.J., Gayral, S., Hampshire, D.J., Ayub, M., Blockmans, M., Pernot, E., Kisseleva, M.V., Compère, P., Schiffmann, S.N., et al. (2009). INPP5E mutations cause primary cilium signaling defects, ciliary instability and ciliopathies in human and mouse. Nat. Genet. *41*, 1027–1031.

Jiang, K., Toedt, G., Montenegro Gouveia, S., Davey, N.E., Hua, S., van der Vaart, B., Grigoriev, I., Larsen, J., Pedersen, L.B., Bezstarosti, K., et al. (2012). A proteome-wide screen for mammalian SxIP motif-containing microtubule plus-end tracking proteins. Curr. Biol. *22*, 1800–1807.

Keady, B.T., Samtani, R., Tobita, K., Tsuchya, M., San Agustin, J.T., Follit, J.A., Jonassen, J.A., Subramanian, R., Lo, C.W., and Pazour, G.J. (2012). IFT25 links the signal-dependent movement of Hedgehog components to intraflagellar transport. Dev. Cell *22*, 940–951.

Kimmel, C.B., Ballard, W.W., Kimmel, S.R., Ullmann, B., and Schilling, T.F. (1995). Stages of embryonic development of the zebrafish. Dev. Dyn. *203*, 253–310.

Koefoed, K., Veland, I.R., Pedersen, L.B., Larsen, L.A., and Christensen, S.T. (2014). Cilia and coordination of signaling networks during heart development. Organogenesis *10*, 108–125.

Kozminski, K.G., Beech, P.L., and Rosenbaum, J.L. (1995). The Chlamydomonas kinesin-like protein FLA10 is involved in motility associated with the flagellar membrane. J. Cell Biol. *131*, 1517–1527.

Kubo, A., Yuba-Kubo, A., Tsukita, S., Tsukita, S., and Amagai, M. (2008). Sentan: a novel specific component of the apical structure of vertebrate motile cilia. Mol. Biol. Cell *19*, 5338–5346.

Laemmli, U.K. (1970). Cleavage of structural proteins during the assembly of the head of bacteriophage T4. Nature *227*, 680–685.

Larkins, C.E., Aviles, G.D., East, M.P., Kahn, R.A., and Caspary, T. (2011). Arl13b regulates ciliogenesis and the dynamic localization of Shh signaling proteins. Mol. Biol. Cell *22*, 4694–4703.

Lawo, S., Hasegan, M., Gupta, G.D., and Pelletier, L. (2012). Subdiffraction imaging of centrosomes reveals higher-order organizational features of pericentriolar material. Nat. Cell Biol. *14*, 1148–1158.

Lechtreck, K.F. (2015). IFT-Cargo Interactions and Protein Transport in Cilia. Trends Biochem. Sci. *40*, 765–778.

Lee, Y.L., Santé, J., Comerci, C.J., Cyge, B., Menezes, L.F., Li, F.Q., Germino, G.G., Moerner, W.E., Takemaru, K., and Stearns, T. (2014). Cby1 promotes Ahi1 recruitment to a ring-shaped domain at the centriole-cilium interface and facilitates proper cilium formation and function. Mol. Biol. Cell *25*, 2919–2933.

Letteboer, S.J., and Roepman, R. (2008). Versatile screening for binary protein-protein interactions by yeast two-hybrid mating. Methods Mol. Biol. *484*, 145–159.

Li, Y., Klena, N.T., Gabriel, G.C., Liu, X., Kim, A.J., Lemke, K., Chen, Y., Chatterjee, B., Devine, W., Damerla, R.R., et al. (2015). Global genetic analysis in mice unveils central role for cilia in congenital heart disease. Nature *521*, 520–524.

Louka, P., Vasudevan, K.K., Guha, M., Joachimiak, E., Wloga, D., Tomasi, R.F., Baroud, C.N., Dupuis-Williams, P., Galati, D.F., Pearson, C.G., et al. (2018). Proteins that control the geometry of microtubules at the ends of cilia. J. Cell Biol. *217*, 4298–4313.

Mahjoub, M.R. (2013). The importance of a single primary cilium. Organogenesis *9*, 61–69.

May-Simera, H.L., and Kelley, M.W. (2012). Cilia, Wnt signaling, and the cytoskeleton. Cilia *1*, 7.

Meier, A., and Söding, J. (2015). Automatic Prediction of Protein 3D Structures by Probabilistic Multi-template Homology Modeling. PLoS Comput. Biol. *11*, e1004343.

Milenkovic, L., Weiss, L.E., Yoon, J., Roth, T.L., Su, Y.S., Sahl, S.J., Scott, M.P., and Moerner, W.E. (2015). Single-molecule imaging of Hedgehog pathway protein Smoothened in primary cilia reveals binding events regulated by Patched1. Proc. Natl. Acad. Sci. USA *112*, 8320–8325.

Mukhopadhyay, S., Wen, X., Chih, B., Nelson, C.D., Lane, W.S., Scales, S.J., and Jackson, P.K. (2010). TULP3 bridges the IFT-A complex and membrane phosphoinositides to promote trafficking of G protein-coupled receptors into primary cilia. Genes Dev. *24*, 2180–2193.

Nachury, M.V. (2018). The molecular machines that traffic signaling receptors into and out of cilia. Curr. Opin. Cell Biol. *51*, 124–131.

Nachury, M.V., Loktev, A.V., Zhang, Q., Westlake, C.J., Peränen, J., Merdes, A., Slusarski, D.C., Scheller, R.H., Bazan, J.F., Sheffield, V.C., and Jackson, P.K. (2007). A core complex of BBS proteins cooperates with the GTPase Rab8 to promote ciliary membrane biogenesis. Cell *129*, 1201–1213.

Nasevicius, A., and Ekker, S.C. (2000). Effective targeted gene 'knockdown' in zebrafish. Nat. Genet. *26*, 216–220.

Pal, K., Hwang, S.H., Somatilaka, B., Badgandi, H., Jackson, P.K., DeFea, K., and Mukhopadhyay, S. (2016). Smoothened determines β-arrestin-mediated removal of the G protein-coupled receptor Gpr161 from the primary cilium. J. Cell Biol. *212*, 861–875.

Patzke, S., Hauge, H., Sioud, M., Finne, E.F., Sivertsen, E.A., Delabie, J., Stokke, T., and Aasheim, H.C. (2005). Identification of a novel centrosome/microtubule-associated coiled-coil protein involved in cell-cycle progression and spindle organization. Oncogene *24*, 1159–1173.

Patzke, S., Stokke, T., and Aasheim, H.C. (2006). CSPP and CSPP-L associate with centrosomes and microtubules and differently affect microtubule organization. J. Cell. Physiol. *209*, 199–210.

Patzke, S., Redick, S., Warsame, A., Murga-Zamalloa, C.A., Khanna, H., Doxsey, S., and Stokke, T. (2010). CSPP is a ciliary protein interacting with Nephrocystin 8 and required for cilia formation. Mol. Biol. Cell *21*, 2555–2567.

Patzke, S., Sternemalm, J., Geimer, S., Sun, X., Aarnes, E., Stokke, T., and Pedersen, L. (2012). Role of CSPP-L in recruitment of ciliopathy proteins to centriolar satellites and the ciliary transition zone. Cilia *1* (*Suppl 1*), P36.

Pedersen, A.G., and Nielsen, H. (1997). Neural network prediction of translation initiation sites in eukaryotes: perspectives for EST and genome analysis. Proc. Int. Conf. Intell. Syst. Mol. Biol. *5*, 226–233.

Ran, F.A., Hsu, P.D., Lin, C.Y., Gootenberg, J.S., Konermann, S., Trevino, A.E., Scott, D.A., Inoue, A., Matoba, S., Zhang, Y., and Zhang, F. (2013). Double nicking by RNA-guided CRISPR Cas9 for enhanced genome editing specificity. Cell *154*, 1380–1389.

Reiter, J.F., and Leroux, M.R. (2017). Genes and molecular pathways underpinning ciliopathies. Nat. Rev. Mol. Cell Biol. *18*, 533–547.

Reiter, J.F., Blacque, O.E., and Leroux, M.R. (2012). The base of the cilium: roles for transition fibres and the transition zone in ciliary formation, maintenance and compartmentalization. EMBO Rep. *13*, 608–618.

Reynolds, E.S. (1963). The use of lead citrate at high pH as an electron-opaque stain in electron microscopy. J. Cell Biol. *17*, 208–212.

Rezabkova, L., Kraatz, S.H., Akhmanova, A., Steinmetz, M.O., and Kammerer, R.A. (2016). Biophysical and Structural Characterization of the Centriolar Protein Cep104 Interaction Network. J. Biol. Chem. *291*, 18496–18504.

Romani, M., Micalizzi, A., and Valente, E.M. (2013). Joubert syndrome: congenital cerebellar ataxia with the molar tooth. Lancet Neurol. *12*, 894–905.

Roosing, S., Hofree, M., Kim, S., Scott, E., Copeland, B., Romani, M., Silhavy, J.L., Rosti, R.O., Schroth, J., Mazza, T., et al. (2015). Functional genome-wide siRNA screen identifies *KIAA0586* as mutated in Joubert syndrome. Elife *4*, e06602.

San Agustin, J.T., Klena, N., Granath, K., Panigrahy, A., Stewart, E., Devine, W., Strittmatter, L., Jonassen, J.A., Liu, X., Lo, C.W., and Pazour, G.J. (2016). Genetic link between renal birth defects and congenital heart disease. Nat. Commun. *7*, 11103.

Sanders, A.A., de Vrieze, E., Alazami, A.M., Alzahrani, F., Malarkey, E.B., Sorusch, N., Tebbe, L., Kuhns, S., van Dam, T.J., Alhashem, A., et al. (2015). KIAA0556 is a novel ciliary basal body component mutated in Joubert syndrome. Genome Biol. *16*, 293.

Sang, L., Miller, J.J., Corbit, K.C., Giles, R.H., Brauer, M.J., Otto, E.A., Baye, L.M., Wen, X., Scales, S.J., Kwong, M., et al. (2011). Mapping the NPHP-JBTS-MKS protein network reveals ciliopathy disease genes and pathways. Cell *145*, 513–528.

Satish Tammana, T.V., Tammana, D., Diener, D.R., and Rosenbaum, J. (2013). Centrosomal protein CEP104 (Chlamydomonas FAP256) moves to the ciliary tip during ciliary assembly. J. Cell Sci. *126*, 5018–5029.

Schindelin, J., Arganda-Carreras, I., Frise, E., Kaynig, V., Longair, M., Pietzsch, T., Preibisch, S., Rueden, C., Saalfeld, S., Schmid, B., et al. (2012). Fiji: an open-source platform for biological-image analysis. Nat. Methods *9*, 676–682.

Schou, K.B., Mogensen, J.B., Morthorst, S.K., Nielsen, B.S., Aleliunaite, A., Serra-Marques, A., Furstenberg, N., Saunier, S., Bizet, A.A., Veland, I.R., et al. (2017). KIF13B establishes a CAV1-enriched microdomain at the ciliary

transition zone to promote Sonic hedgehog signalling. Nat. Commun. *8*, 14177.

Shaheen, R., Shamseldin, H.E., Loucks, C.M., Seidahmed, M.Z., Ansari, S., Ibrahim Khalil, M., Al-Yacoub, N., Davis, E.E., Mola, N.A., Szymanska, K., et al. (2014). Mutations in CSPP1, encoding a core centrosomal protein, cause a range of ciliopathy phenotypes in humans. Am. J. Hum. Genet. *94*, 73–79.

Shearer, R.F., Frikstad, K.M., McKenna, J., McCloy, R.A., Deng, N., Burgess, A., Stokke, T., Patzke, S., and Saunders, D.N. (2018). The E3 ubiquitin ligase UBR5 regulates centriolar satellite stability and primary cilia. Mol. Biol. Cell *29*, 1542–1554.

Shimada, H., Lu, Q., Insinna-Kettenhofen, C., Nagashima, K., English, M.A., Semler, E.M., Mahgerefteh, J., Cideciyan, A.V., Li, T., Brooks, B.P., et al. (2017). In Vitro Modeling Using Ciliopathy-Patient-Derived Cells Reveals Distinct Cilia Dysfunctions Caused by CEP290 Mutations. Cell Rep. *20*, 384–396.

Slaats, G.G., Isabella, C.R., Kroes, H.Y., Dempsey, J.C., Gremmels, H., Monroe, G.R., Phelps, I.G., Duran, K.J., Adkins, J., Kumar, S.A., et al. (2016). MKS1 regulates ciliary INPP5E levels in Joubert syndrome. J. Med. Genet. *53*, 62–72.

Spitzer, M., Wildenhain, J., Rappsilber, J., and Tyers, M. (2014). BoxPlotR: a web tool for generation of box plots. Nat. Methods *11*, 121–122.

Srour, M., Hamdan, F.F., McKnight, D., Davis, E., Mandel, H., Schwartzentruber, J., Martin, B., Patry, L., Nassif, C., Dionne-Laporte, A., et al.; Care4Rare Canada Consortium (2015). Joubert Syndrome in French Canadians and Identification of Mutations in CEP104. Am. J. Hum. Genet. *97*, 744–753.

Sternemalm, J., Geimer, S., Frikstad, K.A., Schink, K.O., Stokke, T., and Patzke, S. (2015). CSPP-L Associates with the Desmosome of Polarized Epithelial Cells and Is Required for Normal Spheroid Formation. PLoS One *10*, e0134789.

Taschner, M., and Lorentzen, E. (2016). The Intraflagellar Transport Machinery. Cold Spring Harb. Perspect. Biol. *8*, a028092.

Thomas, N.A., Koudijs, M., van Eeden, F.J., Joyner, A.L., and Yelon, D. (2008). Hedgehog signaling plays a cell-autonomous role in maximizing cardiac developmental potential. Development *135*, 3789–3799.

Thomas, S., Wright, K.J., Le Corre, S., Micalizzi, A., Romani, M., Abhyankar, A., Saada, J., Perrault, I., Amiel, J., Litzler, J., et al. (2014). A homozygous PDE6D mutation in Joubert syndrome impairs targeting of farnesylated INPP5E protein to the primary cilium. Hum. Mutat. *35*, 137–146.

Torres, J.Z., Miller, J.J., and Jackson, P.K. (2009). High-throughput generation of tagged stable cell lines for proteomic analysis. Proteomics *9*, 2888–2891.

Tuz, K., Bachmann-Gagescu, R., O'Day, D.R., Hua, K., Isabella, C.R., Phelps, I.G., Stolarski, A.E., O'Roak, B.J., Dempsey, J.C., Lourenco, C., et al. (2014). Mutations in CSPP1 cause primary cilia abnormalities and Joubert syndrome with or without Jeune asphyxiating thoracic dystrophy. Am. J. Hum. Genet. *94*, 62–72.

Varshney, G.K., Carrington, B., Pei, W., Bishop, K., Chen, Z., Fan, C., Xu, L., Jones, M., LaFave, M.C., Ledin, J., et al. (2016). A high-throughput functional genomics workflow based on CRISPR/Cas9-mediated targeted mutagenesis in zebrafish. Nat. Protoc. *11*, 2357–2375.

Vierkotten, J., Dildrop, R., Peters, T., Wang, B., and Rüther, U. (2007). Ftm is a novel basal body protein of cilia involved in Shh signalling. Development *134*, 2569–2577.

Waters, A.M., and Beales, P.L. (2011). Ciliopathies: an expanding disease spectrum. Pediatr. Nephrol. *26*, 1039–1056.

Westerfield, M. (2000). The Zebrafish Book. A Guide for the Laboratory Use of Zebrafish (Danio rerio), Fourth Edition (University of Oregon Press).

Yang, T.T., Su, J., Wang, W.J., Craige, B., Witman, G.B., Tsou, M.F., and Liao, J.C. (2015). Superresolution Pattern Recognition Reveals the Architectural Map of the Ciliary Transition Zone. Sci. Rep. *5*, 14096.

Zeng, X., Goetz, J.A., Suber, L.M., Scott, W.J., Jr., Schreiner, C.M., and Robbins, D.J. (2001). A freely diffusible form of Sonic hedgehog mediates long-range signalling. Nature *411*, 716–720.

STAR★METHODS

KEY RESOURCES TABLE

REAGENT or RESOURCE	SOURCE	IDENTIFIER
Antibodies		
Rabbit polyclonal anti-ARL13B	Proteintech	Cat#17711-1-AP; RRID: AB_2060867
Rabbit polyclonal anti-AHI1	Proteintech	Cat#22045-1-AP; RRID: AB_11182927
Rabbit polyclonal anti-IFT88	Proteintech	Cat#13967-1-AP; RRID: AB_2121979
Rabbit polyclonal anti-INPP5E	Proteintech	Cat#17797-1-AP; RRID: AB_2167120
Rabbit polyclonal anti-CEP104	Anna Akhmanova, University of Utrecht, NL	N/A
Rabbit polyclonal anti-CEP97	Proteintech	Cat#22050-1-AP; RRID: AB_11182378
Rabbit polyclonal anti-CP110	Proteintech	Cat#12780-1-AP; RRID: AB_10638480
Rabbit polyclonal anti-CSPP1	Proteintech	Cat#11931-1-AP; RRID: AB_2087897
Mouse monoclonal anti-Chibby	Santa Cruz Biotechnology	Cat#sc-101551; RRID: AB_1561972
Rabbit polyclonal anti-GLI2, H-300	Santa Cruz Biotechnology	Cat#sc-28674; RRID: AB_2111908
Mouse monoclonal anti-SMO	Santa Cruz Biotechnology	Cat#sc-166685; RRID: AB_2239686
Rabbit polyclonal anti-CEP290	Abcam	Cat#ab85728; RRID: AB_1859783
Rabbit polylonal anti-PCM1	Abcam	Cat#ab72443; RRID: AB_1269694
Mouse monoclonal anti-Glutamylated tubulin (GT335)	Adipogen	Cat#AG-20B-0020; RRID: AB_2490210
Mouse monoclonal anti-γ-Tubulin (GTU-88)	Sigma-Aldrich	Cat#T6557; RRID: AB_477584
Donkey polyclonal anti-mouse HRP	Jackson Immunoresearch	Cat#715-035-150; RRID: AB_2340770
Goat polyclonal anti-rabbit HRP	Jackson Immunoresearch	Cat#111-035-144; RRID: AB_2307391
Donkey polyclonal anti-mouse Cy3	Jackson Immunoresearch	Cat#715-165-150; RRID: AB_2340813
Donkey polyclonal anti-rabbit AlexaFluor488	Jackson Immunoresearch	Cat#711-545-152; RRID: AB_2313584
Donkey polyclonal anti-rabbit AlexaFluor647	Jackson Immunoresearch	Cat#711-605-152; RRID: AB_2492288
GFP boost Atto-488	Chromotek	Cat#gba488-100; RRID: AB_2631386
Mouse monoclonal IgG2a anti-CEP104 (G-11)	Santa Cruz Biotechnology	Cat#sc-514475; RRID: AB_2810936
Rabbit monoclonal IgG2a anti-GAPDH (14C10)	Cell Signaling Technology	Cat#2118; RRID: AB_561053
IRDye 680RD goat anti-mouse IgG (H+L)	LI-COR	Cat#926-68070; RRID: AB_10956588
IRDye 800CW goat anti-rabbit IgG (H+L)	LI-COR	Cat#926-32211; RRID: AB_621843
Mouse monoclonal anti-Acetylated tubulin (6-11B-1)	Sigma-Aldrich	Cat#T6793; RRID: AB_477585
Donkey polyclonal anti-mouse AlexaFluor594	Life Technologies	Cat#R37115; RRID: AB_2556543
Rabbit polyclonal anti-aPKC	Santa Cruz Biotechnology	Cat#sc-208; RRID: AB_2168668
Goat polyclonal anti-rabbit AlexaFluor488	Life Technologies	Cat#R37116; RRID: AB_2556544
Chemicals, Peptides, and Recombinant Proteins		
Smoothen Agonist (SAG)	Cayman Chemicals	Cat#11914
Prolong Gold	Life Technologies	Cat#P36930
bisBenzimide H 33258 (Hoechst 33258)	Sigma-Aldrich	Cat#14530
Critical Commercial Assays		
GFP-trap_MA	Chromotek	Cat#gtma-20
Experimental Models: Cell Lines		
Human: hTERT-RPE1	ATCC	Cat#CRL-4000; RRID: CVCL_4388
Human: hTERT-RPE1 CSPP1−/−	This Paper	N/A
Human: hTERT-RPE1 CEP104mut	This Paper	N/A
Human: hTERT-RPE1 WT mNeonGreen-CSPPL	This Paper	N/A
Human: hTERT-RPE1 WT mNeonGreen-CEP104	This Paper	N/A
Human: hTERT-RPE1 CSPP1−/− mNeonGreen-CSPPL	This Paper	N/A

(*Continued on next page*)

Continued

REAGENT or RESOURCE	SOURCE	IDENTIFIER
Human: hTERT-RPE1 CSPP1−/− mNeonGreen-CEP104	This Paper	N/A
Human: hTERT-RPE1 CEP104mut mNeonGreen-CSPPL	This Paper	N/A
Human: hTERT-RPE1 CEP104mut mNeonGreen-CEP104	This Paper	N/A
Human: HEK293T (also called Lenti-X 293T)	Clonetech, Takara Bio Europe	Cat#632180
Experimental Models: Organisms/Strains		
Zebrafish: AB strain	Zebrafish International Resource Center (ZIRC)	Cat#ZL1; RRID: ZIRC_ZL1
Zebrafish: Transgenic *islet-1*:GFP strain (Tg(*isle1*:GFP))	Higashijima et al., 2000	https://www.jneurosci.org/content/20/1/206.long
Zebrafish: Transgenic *cmlc2*:GFP strain (Tg(*cmlc2*:GFP))	Huang et al., 2003	https://doi.wiley.com/10.1002/dvdy.10356
Oligonucleotides		
Morpholino: Intron-Exon splice MO (*cep104* splicing MO) 5′-TGGACAAAACCTACACACAATAGAT-3′	This paper, produced by Gene Tools	N/A
Morpholino: translation blocking (*cep104* ATG MO) 5′-CA CCGTTTGACAACTGTGGCATGTG-3′	This paper, produced by Gene Tools	N/A
Human CEP104 mRNA	This paper	N/A
Primer1 for CRISPR Zebrafish: *cep104* sgRNAs 5′-TTGG CAAGTCAAATGTCTTCTTT-3′	This paper	N/A
Primer2 for CRISPR Zebrafish: *cep104* sgRNAs 5′-GCTG ATGGTAGACTGCGAGT-3′	This paper	N/A
Primer1 for RT.PCR of cep104 splice products in Zebrafish 5′-ATGCCAAAAAGCTGATGGTC-3′	This paper	N/A
Primer2 for RT.PCR of cep104 splice products in Zebrafish 5′-ACCCAACAGCATCAACATGA-3′	This paper	N/A
Recombinant DNA		
pmCherry-CEP104	Jiang et al., 2012	https://linkinghub.elsevier.com/retrieve/pii/S096098221200872X
pEGFP-CEP104 and truncation constructs	Jiang et al., 2012	https://linkinghub.elsevier.com/retrieve/pii/S096098221200872X
pD1401-AP plasmid for CRISPR targeting of *CSPP1* in RPE1 cells with gRNAs: 5′-AATCTGTGAAATCTTCTATC-3′ and 5′-AGGATCGTGTTTTTGATAGA-3′	This paper, (see Figure S5) Produced by DNA2.0	N/A
pD1401-AP plasmid for CRISPR targeting of *CEP104* in RPE1 cells with gRNAs: 5′-AGCTCATCTGGACACGAAGA-3′ and 5′-GTGGGGCATTCTGCACGTTT-3′	This paper, (see Figure S5) Produced by DNA2.0	N/A
ShhN expression plasmid	Bradley Yoder, University of Alabama, USA	http://nature.com/articles/35079648
CSPP-L expression plasmid	Patzke et al., 2010	http://www.molbiolcell.org/doi/10.1091/mbc.E09-06-0503
CSPP-L truncates expression plasmid	Patzke et al., 2010	http://www.molbiolcell.org/doi/10.1091/mbc.E09-06-0503
ARL13B-mCherry plasmid	Kristen J. Verhey, University of Michigan, USA	N/A
IFT-27/IFT-25 expression constructs	Esben Lorentzen, University of Aarhus, DK	N/A
pGLAP3	Addgene	Cat#19704; RRID: Addgene_19704
pENTR20-mNeonGreen-C1	Kay Oliver Schink, Oslo University Hospital, NO	N/A
Lentiviral destination vector derived from pCDH-EF1a-MCS-IRES-Puro (Cat#CD532A-2 from SystemBiosciences)	Kay Oliver Schink, Oslo University Hospital, NO	https://www.biorxiv.org/content/10.1101/180760v2 (preprint)
pMDLg/pRRE (Gag/Pol-plasmid for lentivirus packaging)	Addgene	Cat#12251; RRID: Addgene_12251

(*Continued on next page*)

Continued

REAGENT or RESOURCE	SOURCE	IDENTIFIER
pRSV-Rev (Rev-plasmid for lentivirus packaging)	Addgene	Cat#12253; RRID: Addgene_12253
pMD2.G (VSV-G-plasmid for lentivirus envelope)	Addgene	Cat#12259; RRID: Addgene_12259
Software and Algorithms		
Axiovision 4.8.2	Carl Zeiss	N/A
softWoRx	GE Healthcare	N/A
Fiji/ImageJ	Schindelin et al., 2012	http://www.nature.com/articles/nmeth.2019
SigmaPlot v12.5	Systat Software, Inc	
BoxplotR	Spitzer et al., 2014	http://www.nature.com/articles/nmeth.2811
eggNOG4.5	http://eggnogdb.embl.de/#/app/home Huerta-Cepas et al., 2016	https://academic.oup.com/nar/article/44/D1/D286/250/3059
NCBI	https://www.ncbi.nlm.nih.gov/	N/A
JGI	https://www.jgi.doe.gov/	N/A
Other		
Cover glasses	Hecht Assistent	Cat#1014
35mm ibiTreat μ-culture dishes	Ibidi	Cat#81156

LEAD CONTACT AND MATERIALS AVAILABILITY

Further information and request for reagents should be directed to and will be fulfilled by the Lead Contact, Sebastian Patzke (sebastip@rr-research.no).

EXPERIMENTAL MODEL AND SUBJECT DETAILS

Zebrafish husbandry

All zebrafish procedures were performed under Home Office UK license regulations. We used the zebrafish golden strain, AB strain, the transgenic *islet1*:GFP strain (Tg(*islet1*:GFP) which expresses GFP in cranial motor neurons under the control of islet1 promoter (Higashijima et al., 2000) and the transgenic strain (Tg(*cmlc2*:GFP), expressing the GFP gene under the control of the *cmlc2* promoter (Huang et al., 2003).

METHOD DETAILS

Cell culture and genetic manipulation of hTERT-RPE1 cells

hTERT-RPE1 cells (ATCC #CRL-4000) were maintained in DMEM-F12 medium (Life Technologies, Carlsbad, CA, US) supplemented with 10% Fetal Calf Serum (Life Technologies) and Penicillin/Streptomycin (Sigma-Aldrich, St.Louis, MO, US) in a humidified environment at 37°C and 5% CO_2. For ciliogenesis assays 7x10^4 cells/30 mm well were seeded on coverslips 24h prior to serum withdrawal by two washes with 2 mL pre-warmed serum-free DMEM/F12, and further incubated for 48h. Hh-pathway stimulations were performed on serum starved cells (48h) by addition of 100 nM SAG (Cayman chemical, Ann Arbor, MI, US) at 100 nM (f.c.) or replacement of 1ml medium with ShhN conditioned DMEM (Life Technologies) including 2% Fetal Calf Serum derived from sterile filtered culture supernatants of Hek293T (Clonetech #632180, Takara Bio Europe, Saint-Germain-en-Laye, FR) cells transfected with a ShhN expression plasmid described earlier in (Zeng et al., 2001). Control cells were mock treated with DMSO or Hek293T culture supernatant, respectively. For genetic targeting of *CSPP1* and *CEP104* loci hTERT-RPE1 cells were transfected in at 70% confluence in 10 cm culture dishes with custom made single vectors (DNA2.0, Newark, CA, US) expressing CAS9-D10A (Nickase), Paprika-RFP, and two gene specific gRNA sequences (see Figures S2 and S3 for targeting sequence details). Single transfected cells were isolated by flow cytometry assisted cell sorting on Paprika-RFP expression, individually expanded and 24 monoclonal colonies characterized for target gene and protein expression. Genomic target regions from selected clones were amplified by PCR on genomic DNA using gene specific primers (see Figure S5). PCR products were sub-cloned into pGEM-T vector (Promega) and ten individual clones analyzed by Sanger sequencing using SP6 and T7 directed primers, respectively. Flow cytometry assisted cell sorting and cell cycle analysis was performed as described in (Dale Rein et al., 2015).

Third-generation lentivirus was generated using procedures and plasmids as previously described (Campeau et al., 2009). Briefly, tagged fusions of transgenes were generated as Gateway ENTRY plasmids using standard molecular biology techniques. From

these vectors, lentiviral transfer vectors were generated by Gateway LR recombination into lentiviral destination vectors (Gateway-enabled vectors derived from pCDH-EF1a-MCS-IRES-PURO (SystemBiosciences)). VSV-G pseudotyped lentiviral particles were packaged using a third-generation packaging system (Addgene plasmids #12251, 12253, 12259). Cells were then transduced with low virus titers (multiplicity of infection < 1) and stable expressing populations were generated by antibiotic selection. Detailed cloning procedures are available from the authors.

Plasmids, antibodies and reagents

Plasmids for genetic targeting were acquired from DNA2.0 (Newark, CA, US)). pmCherry-CEP104, pEGFP-CEP104 and pEGFP-CEP104-truncates were described earlier (Jiang et al., 2012). pDEST-GLAP3 was acquired from Addgene (Cambridge, MA, US; (Torres et al., 2009)). Plasmid for expression of soluble Hedgehog ligand (ShhN; (Zeng et al., 2001)) was obtained fromB. K. Yoder (Department of Cell Biology, University of Alabama, USA), the plasmid for expression of mCherry-ARL13B from K. J. Verhey (University of Michigan, USA), and plasmids for IFT25/IFT27 expression from Esben Lorentzen (University of Aarhus, Denmark). CSPP-L and CSPP-L truncate expression plasmids were described earlier (Patzke et al., 2010). All plasmid transfections were performed using Lipofectamine3000 (Life Technologies) according to the protocol from the manufacturer. Detailed information on antibodies are provided in the STAR Methods. Directly Atto488-fluorophore conjugated probes for GFP detection and anti-GFP conjugated paramagnetic beads for immunoprecipitations were from Chromotek (Chromotek GmbH, Munich, DE).

Immunoprecipitations and immunoblotting

Preparation of cell lysates, gel electrophoresis, blotting and immuno-detection was performed as described earlier (Sternemalm et al., 2015). For immunoprecipitation cells were washed thrice in Phosphate buffered saline (PBS; Sigma-Aldrich) and then lysed on ice in cold lysis buffer (50 mM HEPES, pH 7, 150 mM NaCl, 5 mM EDTA, pH 8, 0.1% NP-40, 10% glycerol) supplemented with phosphatase inhibitor cocktails II and III (Sigma-Aldrich) and complete^{TM} protease inhibitor (Roche Diagnostics, Basel, Switzerland). Lysates were collected using a cell scraper, transferred to reaction tubes, left on ice for 20 min for solubilization and then centrifuged at 20.000x*g*/4°C for 15 min. Clarified supernatants were transferred to new reaction tubes for immunoprecipitation using GFP-trap paramagnetic beads (Chromotek GmbH) at 4°C for 2h on a spinning wheel. Beads were washed twice in 500 μl lysis buffer and transferred to a new reaction tube for a third wash. Purified proteins were released from beads and denatured in 40 μl SDS-sample loading buffer and 5 min incubation at 95°C.

Immunofluorescence and live cell microscopy

Cells were grown on heat-sterilized cover glasses (No.1014; Glaswarenfabrik Karl Hecht GmbH & Co KG, Sondheim/Rhön, DE), fixed for 15 min in 1% neutral buffered formalin solution at room-temperature prior to post-fixation in methanol (−20°C). Cells were re-hydrated for IFM staining by three consecutive washes in PBS and blocked and permeabilized for 30 min in PBS-AT (PBS containing 5% wt/vol Bovine serum albumin (BSA) and 0.1% vol/vol Triton X-100). Cells were stained with primary antibodies for 2h at room temperature, washed thrice in PBS, and stained with secondary antibodies for 45 min. All antibody incubations were performed in PBS-AT. Cells were washed thrice in PBS, counterstained for DNA (Hoechst 33258 in PBS, Sigma), washed briefly in distilled water, dried and mounted on object glasses using Prolong Gold (Life Technologies). Fluorescence images were acquired using appropriate optical filters on a multi-fluorescent bead calibrated AxioImager Z1 ApoTome microscope system (Carl Zeiss, Jena, DE) equipped with a 100x or a 63x lens (both PlanApo N.A.1.4) and an AxioCam MRm camera. To display the entire cell volume, images are presented as maximal projections of z stacks using Axiovision 4.8.2 (Carl Zeiss).

3D-SIM imaging was performed using a Deltavision OMX V4 microscope (GE Healthcare, Little Chalfont, UK) equipped with three water-cooled PCO.edge sCMOS cameras, 405 nm, 488 nm, 568 nm and 642 nm laserlines and a 60x 1.42NA Plan-Apochromat lense (Olympus, Tokyo, JP). z stacks covering the whole cell, with sections spaced 0.125 mm apart, were recorded. For each z section, 15 raw images (three rotations with five phases each) were acquired and the final super-resolution images were reconstructed using softWoRx software (GE Healthcare).

Images for quantitative IFM imaging were acquired on a multi-fluorescence sub-micron beads calibrated CellObserver microscope system (Carl Zeiss) equipped with a 40 × /1.3 PlanApo Phase 3 lens and an AxioCam MRm camera. Images were acquired with constant exposure times at 10 random positions per coverslip and in seven optical sections at 0.5 μm distance, centered around focal planes for cilia. Focal planes were identified by glutamylated tubulin or ARL13B labeling as cilia reference, respectively, using a contrast based autofocus routine (AxioVision 4.8.2). Image analysis was performed in Fiji/ImageJ (Schindelin et al., 2012). Sum projections of individual channels were background corrected using a 5px rolling circle algorithm and cilia segmented in cilia reference channels by signal intensity and morphological thresholds to create cilia masks. Fluorescence signal intensities under each mask were measured in all channels and median signal intensities determined.

All statistical analysis was performed using t test analysis tool in SigmaPlot v12.5 (Systat, Inc., San Jose, CA,US) and boxplots created in BoxplotR (Spitzer et al., 2014).

For live cell microscopy cells were grown in 35-mm ibiTreat μ-culture dishes (Ibidi, Munich, DE) and imaged using a CellObserver microscope system (Carl Zeiss) equipped with a 40 × /1.3 PlanApo Phase 3 lens, a Hamamatsu ORCA-Flash4.0 v3 camera, a temperature controlled XL-chamber, a temperature, humidity and CO_2 controlled stage incubator, a motorized coded X,Y-stage, a Definite Focus system and a HXP120 Metal-Halide illumination unit.

Post-embedding immunogold electron microscopy

Small pieces (about 2 mm^2) of mouse trachea were fixed in MT-buffer (30 mM HEPES, 5 mM Na-EGTA, 15 mM KCl, pH 7.0) containing 3.5% formaldehyde for 2–3 h at 4°C. After two brief washes with MT-buffer the tissue was dehydrated to 100% ethanol (30% and 50% ethanol on ice; then 70%, 95%, 100% ethanol at −20°C, 15 min each). Infiltration of the samples with LR Gold resin (London Resin Company, Reading, GB) was performed at −20°C according to the following scheme: LR Gold/ethanol (1:3) for 2 h, LR Gold/ethanol (3:1) for 4 h, LR Gold containing 0.4% benzil for 36 h (with several changes of the medium). Polymerization was performed under fluorescent light for 48 h at −20°C. Ultrathin sections (60-80 nm) were cut with a diamond knife (type ultra 35°; Diatome, Biel, CH) on a EM UC6 ultramicrotome (Leica Microsystems, Wetzlar, DE) and mounted on pioloform-coated, single-slot gilded copper grids (Science Services, Munich, DE). For immunolabeling, the sections were blocked for 1-2 h at room temperature with blocking buffer (2% BSA, 0.1% fish gelatin and 0.05% Tween 20 in PBS; pH 7.4) and incubated in anti-CSPPL antibody (polyclonal, rabbit, diluted 1:200 or 1:1000 in blocking buffer) overnight at 4°C. Grids were washed 3-5 times with PBS containing 0.15% BSA-c (Aurion, Wageningen, NL) for 10 min each and incubated for 1.5 h with 15-nm gold particles conjugated to goat anti-rabbit IgGs (British Biocell, Cardiff, GB) diluted 1:30 in blocking buffer. Grids were washed 3-5 times with PBS containing 0.15% BSA-c for 10 min each, fixed for 8 min in 1% glutaraldehyde in PBS and washed 3 times for 5 min each in distilled water. After immunolabeling, the sections were stained with uranyl acetate and lead citrate (Reynolds, 1963) and viewed with a JEM-2100 transmission electron microscope (JEOL, Tokyo, JP) operated at 80 kV. Micrographs were taken using a 4,080 × 4,080 pixels charge-coupled device camera (UltraScan 4000, Gatan, Pleasanton, CA, US) and Gatan Digital Micrograph software (version 1.70.16). Image brightness and contrast were adjusted using Adobe Photoshop 8.0.1.

Direct yeast two-hybrid interaction assay, sucrose density fractionation and size exclusion chromatography

The direct interaction between CSPP-L and other ciliary proteins was tested using a GAL4-based yeast two-hybrid system, with yeast strain PJ69-4A and PJ69-4α, using general procedures for yeast mating described previously (Letteboer and Roepman, 2008). In brief, a construct encoding full-length CSPP-L, fused to either a DNA-binding domain (GAL4-BD), or to a transcription activating domain (GAL4-AD) were used to screen a gridded library of cDNA clones, expressing different ciliary and/or ciliopathy-associated proteins, fused to GAL4-AD or GAL4-BD, respectively. The direct interaction between baits and preys induced the activation of the reporter genes, resulting in the growth of yeast colonies on selective media (deficient of Leu, Trp, His, and Ade) and induction of α-galactosidase and β-galactosidase colorimetric reactions. Positive clones were subsequently validated by co-transformation of the cognate plasmids, and growth selection on media lacking His, Leu, and Trp, supplemented with 10 mM 3-AT. For density fractionation 200μl total cell lysate was loaded onto a continuous 10%–60% sucrose gradient prepared by mixing 60 and 10% sucrose solutions (5.5 mL of each) using a Biocomp Gradient Master (BioComp Instruments, Fredericton, CA) and centrifuged at 100.000xg for 16 h at 4C in a SW-40Ti rotor (Beckman-Coulter, Pasadena, CA, US). Procedures for size exclusion chromotography have been published previously (Schou et al., 2017).

Zebrafish genetic manipulation

All zebrafish procedures were performed under Home Office UK license regulations. Zygotes were collected from natural spawning and placed in Petri dishes of E3 medium (Westerfield, 2000). Zebrafish embryos were collected and raised at 28.5 °C and staged in somite stage and hpf according to standard criteria (Kimmel et al., 1995). Antisense morpholino oligonucleotides (MOs) were designed (Gene Tools, Philomath, Oregon, US) to target zebrafish *cep104* (XP_003199125.2) as follows: Intron-Exon splice MO (*cep104* splice MO): 5′-TGGACAAAACCTACACACAATAGAT-3′; translation blocking (*cep104* ATG MO): 5′-CACCGTTTGA CAACTGTGGCATGTG-3′. Stock MOs in RNase free water were diluted with 0.05% phenol red in Danieau buffer (Nasevicius and Ekker, 2000) to produce the solution for injection. Escalating doses of each MO were tested for phenotypic effects. Embryos were injected with 0.8 pmol/embryo of *cep104* splicing MO or 0.8 pmol/embryo of *cep104* ATG MO at 1- to 2-cell stage. For combined knockdown experiments, 0.8 pmol/embryo of each MO was used. For rescue experiments, morpholino was co-injected with 250 pg/embryo of *CEP104* mRNA.

Protein extraction and immunoblotting on zebrafish samples

Whole protein extracts were obtained from 48 hpf de-yolked zebrafish embryos by mechanical desegregation of the embryos into Laemmli sample buffer (Laemmli, 1970). Samples were incubated at 98°C for 5 min and resolved by SDS-PAGE. Proteins were transferred to a nitrocellulose membrane (Thermo Fisher). The membranes were incubated with the following antibodies: mouse monoclonal IgG2a anti-CEP 104 (G-11), (sc-514475, SCBT), rabbit monoclonal IgG2a anti-GAPDH (14C10), (2118, Cell Signaling Technology), IRDye® 680RD goat anti-mouse IgG (H + L), (926-68070, LI-COR, Lincoln, NE, US), IRDye® 800CW goat anti-rabbit IgG (H + L), (926-3221, LI-COR). Protein signals were then detected using the ODYSSEY CLx (LI-COR) imaging system.

Kupffer's vesicle imaging

Uninjected and *cep104* MO injected zebrafish embryos were fixed at the 10 somite stage, using 4% paraformaldehyde in PBS at 4°C overnight. To permeabilise, embryos were washed in ddH20 then pre-chilled acetone (−20°C) for 7 min. Embryos were washed in ddH_2O and blocked in 5% BSA, with 1% DMSO and 0.1% Tween. For cilia staining, embryos were incubated in primary antibody (mouse anti-acetylated tubulin antibody, 1:500, Sigma T6793) overnight at 4°C and detected using a donkey anti-mouse

AlexaFluor594 conjugated secondary antibody (1:300, Life Technologies). For identification of KV epithelium, antibodies directed toward aPKC were used (rabbit anti-aPKC (1:500, SCBT) detected with goat anti-rabbit Alexa Fluor 488 conjugated secondary antibody (1:300, Life Technologies). Embryos were washed into PBS, mounted and imaged using an Axio Imager Z1 fluorescence microscope (Zeiss).

Zebrafish husbandry and genetic manipulation

The *cep104* sgRNA was designed using https://www.crisprscan.org/ to target the following region of *cep104* gene: 5′-GGTGGGCGAACGGTTGGGC-3′. sgRNA and Cas9 protein (NEB) were solubilized with 300 mM KCl and diluted in 0.05% phenol red in RNase free water at final concentration of respectively 300ng/ul and 4uM and were injected into 1-cell stage embryos. Zebrafish were anaesthetized with Tricaine solution and phenotyped at 48 hpf. Images were captured using a fluorescent stereomicroscope (Leica MZ16F). sgRNA was synthesized using a cloning-free, oligo-based method (Varshney et al., 2016). *In vitro* transcription was carried out using MEGAshortscript T7 transcription kit (Thermo Fisher). sgRNA was then purified with mirVana Isolation Kit (Thermo Fisher). To check the specificity and efficiency of genome editing, 11 embryos from a sample population of F0 animals were genotyped by amplifying surrounding region of targeted *cep104* sequence, using gene-specific primer pairs (5′-TTGGCAAGT CAAATGTCTTCTTT-3′and 5′-GCTGATGGTAGACTGCGAGT-3′). Amplification product from each F0 crispant embryos was then sequenced and compared to amplification product from uninjected embryos to screen for mutations.

Zebrafish RNA isolation and RT-PCR

Total RNA was isolated from single zebrafish embryos at 48 hpf. RNA was used for each experimental group in reverse transcription (RT) reactions. Superscript VILO cDNA synthesis kit (Life Technologies) was used for RT. PCR using gene-specific primer pairs (5-ATGCCAAAAAGCTGATGGTC-3 and 5-ACCCAACAGCATCAACATGA-3) was performed to identify splice products following *cep104* splice MO injection.

Pronephros imaging

For pronephros imaging, uninjected and *cep104* MO or CRISPR/Cas9- injected embryos were fixed at 72 hpf with 4% paraformaldehyde in PBS at 4°C overnight. To permeabilise embryos they were washed in ddH20 then pre-chilled acetone (−20°C) for 7 min. Embryos were washed in ddH2O, treated with collagenase A (Roche) at 1mg/ml in PBS-Tween 0.1% for 30' at room temperature and blocked in 5% horse serum in PBS-Tween 0.1% for 1 h at room temperature. For cilial staining, embryos were incubated in primary antibody (mouse anti-acetylated tubulin antibody, 1:500, Sigma T6793) overnight at 4°C and detected using a donkey anti-mouse AlexaFluor594 conjugated secondary antibody (1:400, Life Technologies). Embryos were washed into PBS and imaged using confocal microscopy (A1R Confocal, Nikon).

Evolutionary and comparative structure analysis

Putative CEP104 and CSPP1 orthologs were identified using a combination of reciprocal best BLASTP and iterative BLASTP as simple BLAST searches. Protein sequences were used to query the non-redundant predicted proteomes of flagellate and non-flagellate organisms, chosen to represent a wide evolutionary spread of eukaryotes. Searches were carried out at eggNOG4.5 (Huerta-Cepas et al., 2016), NCBI (https://www.ncbi.nlm.nih.gov/) or JGI (https://www.jgi.doe.gov/) depending on the organism. Comparative structure analysis was carried out at HHPred (Hildebrand et al., 2009).

QUANTIFICATION AND STATISTICAL ANALYSIS

Statistical analysis were performed using SigmaPlotv12.5 (SysStat). Statistical details of experiments are stated in the legends of figures displaying the respective data, including the statistical tests used, the number of replicates and number of investigated cells/fish, measures of precision and definitions of significance.